UNIVERSITEIT VAN PRETORIA
UNIVERSITY OF PRETORIA
YUNIBESITHI YA PRETORIA

UNIVERSITY OF PRETORIA

Experimental and Numerical investigation into the natural convection of TiO_2-Water nanofluid inside a cavity

by Tanja Linda Ottermann

Submitted in partial fulfillment of the requirements for the degree

Master of Engineering (Mechanical Engineering)

In the Department of Mechanical and Aeronautical Engineering,
Faculty of Engineering, Built Environment and Information Technology

University of Pretoria

November 2016

Abstract

Title: Experimental and Numerical investigation into the natural convection of TiO_2-Water nanofluid inside a cavity

Supervisor: Dr Mohsen Sharifpur and Prof Josua Meyer

Department: Mechanical and Aeronautical Engineering

Degree: Master of Engineering (Mechanical Engineering)

This Master of Engineering investigation focuses on the natural convection of nanofluids in rectangular cavities. The governing equations applied to analyse the heat transfer and fluid flow occurring within the cavity are given and discussed. Special attention is given to the models that were developed to predict the thermal conductivity and dynamic viscosity of such nanofluids.

A review concerning past investigations into the field of natural convection of nanofluids in cavities is made. The investigation is divided into experimental works and computational fluid dynamics (CFD) numerical investigations.

Through the literature review, it was discovered that many numerical models exist for the prediction of the thermophysical properties of nanofluids, specifically thermal conductivity and viscosity. Depending on the nanofluid and the application, different models can be used.

The literature study also revealed that most previous works were done in the CFD field. Very few experimental studies have been performed. Numerical CFD investigations, however, need experimental results for validation purposes, leading to the conclusion that more experimental work is needed.

The heat transfer capability and thermophysical properties of the nanofluid are investigated based on models found in literature. The investigation incudes measuring the heat transfer inside a cavity filled with a nanofluid and subjected to a temperature gradient. The experiment is performed for several volume fractions of particles. An optimum volume fraction of 0.005 is obtained. At this volume fraction the heat transfer enhancement reaches a maximum for the present investigation.

The investigation is repeated as a numerical investigation using the commercially available CFD software ANSYS-FLUENT. The same case as used in the experimental investigation is modelled as a two-dimensional case and the results are compared. The same optimum volume fraction and maximum heat transfer is obtained with an insignificantly small difference between the two methods of investigation. This error can be attributed to the minor heat losses experienced from the experimental setup as in the CFD adiabatic walls considered.

It is concluded that, through the inclusion of TiO_2 particles in the base fluid (deionised water), the thermophysical properties and the heat transfer capability of the fluid are altered. For a volume fraction of 0.005 and heat transfer at a temperature difference of 50 °C, the heat transferred through the fluid in the cavity is increased by more than 8%.

From the results, it is recommended that the investigation is repeated with TiO_2 particles of a different size to determine the dependency of the heat transfer increase on the particle size. Various materials should also be tested to determine the effect that material type has on the heat transfer increase.

Keywords: *Nanofluid, natural convection, experimental, cavity, numerical, titanium dioxide, volume fraction*

Acknowledgements

I would like to acknowledge my supervisor, Dr Mohsen Sharifpur, for his guidance throughout my master's research, Dr Brusly Solomon for his contributions during the experimental investigation, and my co-supervisor, Prof Josua Meyer, for his and the department's support. Special acknowledgement also goes to the laboratory staff of the University of Pretoria and the Council for Scientific and Industrial Support (CSIR) for their assistance.

A special thank you also goes out to my family and friends for their continued support during the completion of my studies.

Table of contents

List of figures

List of tables

Nomenclature

g	Gravitational acceleration (m^2/s)
T	Temperature (°C or K)
L/l	Length (m)
H	Height (m)
W	Width (m)
t	Time (s)
K_B	Boltzmann constant
N_A	Avogadro's constant
G_T	Total interparticle potential
m	Mass (kg)
k	Thermal conductivity (W/m K)
h	Heat transfer coefficient (W/m^2K)
q	Heat transfer (W)
C_p	Specific heat constant (J/kg K)
C_f	Heat capacity per unit volume of fluid (J/m^3K)
D/d	Diameter (m)
R	Radius (m)
u	Velocity – x direction (m/s)
v	Velocity – y direction (m/s)
r_c	Cluster radius (m)

Dimensionless parameters

Ri	Richardson number
Ra	Rayleigh number
Gr	Grashof number
Pr	Prandtl number
Re	Reynolds number
Nu	Nusselt number

Greek symbols

α	Thermal diffusivity (m^2/s)
β	Thermal expansion coefficient
μ	Dynamic viscosity (kg/ms)
ρ	Density (kg/m^3)
ζ	Zeta potential (mV)
η	Intrinsic viscosity
ν	Kinematic viscosity (m^2/s)
φ	Volume fraction (%)

Subscripts

bf	Base fluid
f	Fluid
nf	Nanofluid
eff	Effective
p	Particle
h	Hot
c	Cold/critical
s	Surface
∞	Ambient
0	Initial
EDL	Electrical double layer
nl	Nanolayer
x	X-direction
y	Y-direction
fr	Freezing point
pn	Nanoparticle

Publications

From the research done in this investigation, the following articles were produced:

Articles for international journals:

- A.B. Solomon, M. Sharifpur, Tanja Ottermann, Carla Grobler, Michael Joubert and J.P. Meyer, *Natural convection enhancement in a porous cavity with Al203-Ethylene Glycol/water nanofluids,* International Journal of Heat and Mass transfer, Vol. 108, Part B, May 2017, pp. 1324-1334.

- T.L. Ottermann, M. Sharifpur and J.P. Meyer*, Experimental investigation into the natural convection heat transfer capabilities of TiO_2 – water nanofluids,* prepared to be submitted to Experimental Thermal and Fluid Science.

Articles for international conference:

- T.L. Ottermann, M. Sharifpur and J.P. Meyer, *Numerical investigation into the heat transfer capabilities of TiO_2 – water nanofluid and a comparison to the experimental results,* prepared to be submitted to 13th International Conference on Heat Transfer, Fluid Mechanics and Thermodynamics (HEFAT 2017).

1. Introduction

This section provides and introduction to the background of the investigation, along with its importance and the problem statement, aim, objectives and methodology.

1.1 Background

The fluids that are usually used as heat transfer fluids have limited capacity to remove heat in various heat exchange processes. The progression of the technology has resulted in an explosive growth in thermal management problems in compact spaces. Nanofluids, which are solid-liquid composites, show higher thermal conductivity and higher convective heat transfer performance than liquids traditionally used. Therefore, by using nanotechnology, the heat transfer process can be optimised. These nanoparticles, which are suspended in the fluids, can be ceramics, oxides, metals and nanotubes with sizes that usually vary between 1 to 100 nm. The most important parameters in thermal fluid analyses of nanofluids are effective thermal conductivity, effective viscosity and the conditions that improve the convective heat transfer by using such fluids.

The research will summarise the existing investigations into nanofluids and the models that can be used to represent their properties. From the existing research, the most suited models will be used to represent the chosen nanofluid, titanium dioxide (TiO_2) in deionised water. Various volume fractions of the nanofluid will be investigated experimentally and a numerical investigation will be performed. The numerical investigation will be used for validation and comparison purposes

From the experimental and numerical investigation the optimum volume fraction for the selected case will be obtained.

1.2 Importance

The importance of the proposed investigation lies in the fact that the full use of nanofluids and their specific properties is currently not fully comprehended. Through the research, an informed decision was made on what nanofluid the research should focus on. The experimental investigation is conducted with the aim of finding the optimum volume fraction of nanoparticle for which the maximum heat transfer rates would be achieved. A numerical investigation was used to validate and compare the experimental results.

The proposed research is of importance as it provides a better understanding of the effects the addition of nanoparticles to fluids have on their heat transfer capability.

1.3 Problem statement

Due to the advantages of nanofluids compared with conventional heat transfer fluids, nanofluids – as heat transfer fluids – have received significant attention in past years. However, there are still problems in modelling and predicting the thermophysical properties of nanofluids. Many factors affect the thermophysical properties of these new fluids, including nanoparticle type, shape, size, temperature, volume fraction of particles and the nanofluid's preparation method. In this research, past investigations will be analysed, after which an investigation will be proposed. The investigation will include an experimental aspect, as well as a numerical investigation, and a subsequent

comparison and recommendations. From the investigation into existing literature on nanofluids, a nanofluid is selected that is investigated experimentally and numerically.

1.4 Aim

The aim of this dissertation is to investigate what research has been done in the field of natural convection and nanofluids. The different models that have been developed to determine nanofluid properties are to be summarised. From this information, an investigation into the heat transfer capabilities and thermophysical properties of a specific nanofluid is to be done. The investigation should contain experimental, as well as numerical components.

1.5 Objectives

The first objective for the investigation is to summarise and analyse the available models for the prediction of the thermophysical properties of nanofluids. The second objective is to determine what research has been conducted on which nanofluids and then to propose a new investigation into a specific nanofluid and its properties. From the investigation into existing literature, an experimental and numerical investigation into a selected nanofluid will be set up and conducted. The main objective of the investigation is to determine the optimum volume fraction and temperature difference at which this nanofluid has the maximum heat transfer.

1.6 Dissertation methodology

Chapter 1: Introduction

Background of the research, importance of the research, problem statement of the dissertation, aim and objectives of the master's dissertation.

Chapter 2: Literature study

Background of basic fluid mechanics, theory behind natural convection, detailed discussion of nanofluids and the models available to determine their properties, discussion of past experimental and numerical works.

Chapter 3: Experimental investigation

An experimental investigation into a TiO_2 deionised water nanofluid. Selecting the models or methods used to determine the nanofluid's thermophysical properties. Obtaining the optimum volume fraction for maximum heat transfer through the use of a carefully designed experimental procedure.

Chapter 4: Numerical investigation

A numerical investigation into the heat transfer capability of the chosen nanofluid, using commercial computational fluid dynamics (CFD) software (ANSYS-FLUENT) to validate the experimental results.

Chapter 5: Conclusion and recommendation

Concluding the investigation by summarising the various sections of the investigation and the related results, and providing recommendations.

2. Literature study

2.1 Introduction to the literature study

This chapter summarises a few fundamental concepts that are key to the concepts of natural convection in nanofluids. The chapter also briefly explores the governing equations and relevant numerical models needed to analyse natural convection. A general overview of the previous works in the field of the natural convection of nanofluids, specifically cavity flow, is also provided.

2.2 Natural convection

The following section deals with natural convection. The general governing equations are provided, along with a short explanation of natural convection.

Convection is the mode of heat transfer between a solid surface and the adjacent liquid or gas that is in motion. It involves the combined effects of conduction and fluid motion. Natural convection, also known as free convection, is the type of convection where the fluid flow is caused by buoyancy forces within the fluid [1].

2.2.1 Governing equations

The governing equations are rederived by Çengel and Ghajar [1] for natural convection in two dimensions. The mass and energy equations are derived for forced convection hold, with the equation of motion having to be re-defined. The governing equations for natural convection are thus defined as [1]:

Continuity equation:

$$\frac{\partial u}{\partial x} + \frac{\partial v}{\partial y} = 0 \tag{1}$$

Momentum equation:

$$u\,\frac{\partial u}{\partial x} + v\,\frac{\partial u}{\partial y} = v\,\frac{\partial^2 u}{\partial y^2} + g\beta(T - T_\infty) \tag{2}$$

Energy:

$$u\,\frac{\partial T}{\partial x} + v\frac{\partial T}{\partial y} = \alpha\,\frac{\partial^2 T}{\partial y^2} \tag{3}$$

Where β is the volume expansion coefficient of the fluid and α is the thermal diffusivity (m^2/s).

With the boundary conditions:

$$at\ y = 0:\ u(x,0) = 0, \qquad v(x,0) = 0, \qquad T(x,0) = T_s \tag{4}$$

$$at\ y \to \infty:\ u(x,\infty) \to 0, \qquad v(x,\infty) \to 0, \qquad T(x,\infty) \to T_\infty \tag{5}$$

2.2.2 Non-dimensional parameters

Through non-dimensionalising the governing equations, dimensionless parameters are obtained. The typical scales that are used to non-dimensionalise the governing equations are: characteristic length, characteristic velocity, characteristic time scale, characteristic pressure and characteristic temperature. These parameters represent the natural convection effects.

The Grashof number is a measure of the ratio between the buoyancy and viscous forces and is defined as:

$$Gr = \frac{g\beta(T_s - T_\infty)L_c^3}{\nu^2} \tag{6}$$

Another important non-dimensional parameter is the Richardson number, which is a measure of the buoyancy force and the flow gradient, given as:

$$Ri = \frac{Gr}{Re^2} \tag{7}$$

The flow gradient is a result of the buoyancy forces which in turn result from the temperature gradient. Although not used in this thesis, it is a valid and interesting way to represent the effects of natural convection.

The Rayleigh number is a product of the Grashof number and the Prandtl number and describes the ratio between buoyancy forces, and thermal and momentum diffusivities. The Rayleigh number is defined as:

$$Ra = Gr\,\mathrm{Pr} = \frac{g\beta(T_s - T_\infty)L_c^3}{\nu\alpha} \tag{8}$$

2.3 Nanofluids

This section of the literature study contains an overview of nanofluids and the models used to approximate their properties.

2.3.1 Background to nanofluids

A nanofluid is a type of fluid that can be used for heat transfer in engineering applications. Nanofluids are comprised of a base fluid (e.g. water) that has nano-sized particles (e.g. Al_2O_3) suspended in it [2].

By suspending nanoparticles with a higher thermal conductivity than the base fluid within the fluid, the heat transfer capabilities of the fluid are enhanced. The nanoparticles have thus altered the properties of the fluid.

2.3.2 Methods of producing nanofluids

Two methods exist for producing nanofluids.

The first method is the one-step direct evaporation method. This method involves the direct formation of the nanoparticles inside the base fluid [2].

The second method is the two-step method. This method represents the formation of nanoparticles and the subsequent dispersion of the nanoparticles in the base fluid. With this method, the nanoparticles are produced separately, after which the particles are dispersed in the base fluid. To ensure homogenous dispersion, the fluid must be treated. Types of treatment devices that are currently being used include the stirrer, the ultrasonic bath, the high-pressure homogeniser and the ultrasonic disruptor. The methods are used to prevent the formation of clusters within the produced nanofluid [2].

Either method can be used to produce nanofluids.

2.3.3 Stability of nanofluids

When conducting experiments, it is important that the nanofluid is stable throughout the study, as the stability can affect the data. A stable nanofluid is defined by Meyer, Adio, Sharifpur and Nwosu [3] to be when nanoparticles are continually in their Brownian motions without cohesion and devoid of flocculation, agglomeration and ultimately sedimentation.

The durations of the period during which a nanofluid is stable can be described as a function dependent on various components. These include nanoparticle type, particle volume concentration, type and concentration of surfactant, shape of particle, type of system (stationary or dynamic), temperature of suspension, method of preparation and density difference between the nanoparticles and the base fluid [3].

Different methods exist with which the stability can be investigated. Methods such as visual inspection for sedimentation, sedimentation rate measurement, turbidity, zeta potential, absorbency of nanofluids and transmittance are among the most commonly used [3]. Most of these methods, however, have restrictions to their use.

2.3.4 Natural convection within a cavity filled with a nanofluid

To analyse the heat transfer and flow of nanofluids, the general equations are modified to incorporate the specific properties of the nanofluid. This section modifies the equations for the case of natural convection within a cavity filled with a nanofluid.

The governing equations are altered to become (assuming two-dimensional):

Continuity equation:

$$\frac{\partial u}{\partial x} + \frac{\partial v}{\partial y} = 0 \tag{9}$$

Momentum equation (x-direction):

$$u\frac{\partial u}{\partial x}+\ v\frac{\partial u}{\partial y}=\frac{1}{\rho_{nf}}\left(-\frac{\partial p}{\partial x}+\mu_{nf}\nabla^2 u+(g\beta)_{nf}g_x(T-T_c)\right) \tag{10}$$

Momentum equation (y-direction):

$$u\frac{\partial v}{\partial x}+\ v\frac{\partial v}{\partial y}=\frac{1}{\rho_{nf}}\left(-\frac{\partial p}{\partial y}+\mu_{nf}\nabla^2 v+(g\beta)_{nf}g_y(T-T_c)\right) \tag{11}$$

Energy equation:

$$\frac{\partial T}{\partial t}+\ u\frac{\partial T}{\partial x}+v\frac{\partial T}{\partial y}=\frac{1}{\rho_{nf}c_{p,nf}}\left[\frac{\partial}{\partial x}\left(k_{eff}\frac{\partial T}{\partial x}\right)+\frac{\partial}{\partial y}\left(k_{eff}\frac{\partial T}{\partial y}\right)\right] \tag{12}$$

The non-dimensional parameters are also modified. The Rayleigh number is calculated using the equation:

$$Ra=\frac{g\rho_{nf}c_p\beta_{nf}(T_h-T_c)l^3}{k_{nf}\mu_{nf}} \tag{13}$$

The Nusselt number is calculated with:

$$Nu=\frac{hl}{k_{nf}} \tag{14}$$

where

$$h=\frac{q}{(T_h-T_c)} \tag{15}$$

Using the above equation, the heat transfer and fluid flow of the nanofluid can be analysed. The material-specific properties, viscosity, thermal conductivity, thermal expansion coefficient, density and specific heat capacity, are needed for the analysis.

2.3.5 Predicting the thermophysical properties of nanofluids

As nanofluids have properties that are dependent on the base fluid and the added particles, methods are needed to approximate the properties. The methods available to predict thermal conductivity and viscosity are discussed in this section.

2.3.5.1 Viscosity of nanofluids

To analyse the efficiency of a heat transfer system that includes a nanofluid, the viscosity of the fluid is extremely important. Nanoparticles suspended in a base fluid produce increased heat transfer capabilities, but also an increase in the viscosity. The viscosity plays an important role in the pumping power required, an increase of which would result in a decrease of the overall efficiency.

Theoretical and empirical models exist that can be used to determine the viscosity of a nanofluid. Meyer et al. [3] executed a review of the available models. These models are presented in the following categories: classical theoretical models, new theoretical models and empirical models.

Classical theoretical models

As these models were developed prior to the research into nanofluids. Most of them have limited applications in the field of nanofluids. The models are discussed below.

The standard model of Einstein [4] is based on infinite dilute suspensions of uncharged hard spheres. This was the first prediction for the viscosity of a nanofluid. The model is described by the equation:

$$\mu_{eff} = \mu_{bf}(1 + [\eta]\emptyset) \tag{16}$$

where η is the intrinsic viscosity of the suspension, equal to 2.5 for hard spheres. The model is valid for volume fractions below 2%.

Smoluchowski [5] presented a model that, contrary to Einstein's model, predicted the effective viscosity for charged particles in electrolyte suspension. The model is given as:

$$\mu_{eff} = \mu_{bf}\left[1 + 2.5\emptyset\left\{1 + \frac{1}{k\mu_{bf}a^2}\left(\frac{\zeta D_E}{2\pi}\right)^2\right\}\right] \tag{17}$$

With the specific conductivity of the electrolyte (k), radius of the solid particles (a), dielectric constant of the water (D_E) and the zeta potential of the particle with respect to the electrolytic medium (ζ).

Booth [6] stated that the Smoluchowski model included overpredictions and subsequently proposed a model that showed good agreement to the experimental data produced by Bull [7] . The model is given as:

$$\mu_{eff} = \mu_{bf}\left[1 + 2.5\emptyset\left\{1 + \sum_{1}^{\infty} b_I\left(\frac{e\zeta}{K_B T}\right)^I\right\}\right] \tag{18}$$

with b_I being the characteristics of the electrolyte and e the electronic charge on particles.

Many researches extended the Einstein model to be valid for specific conditions. Such models are discussed below.

Taylor [8] extended the model for liquid drops suspended in another liquid. Vand [9] also proposed an extended model.

The extended model of Brinkman [10] is valid for volume fractions below 0.04 and is described as:

$$\mu_{eff} = \mu_{bf}(1 + \emptyset)^{-2.5} \tag{19}$$

While Mooney [11] presented a semi-empirical model limited to rigid spherical particles, Roscoe [12] developed a model for spheres of equal size and high concentrations.

Batchelor [13] proposed a model accounting for the influence of interparticle interactions for volume fractions below 0.04. The model is given as:

$$\mu_{eff} = \mu_{bf}(1 + [\eta]\emptyset + k_H([\eta]\emptyset)^2) \tag{20}$$

where k_H is the Huggins coefficient (interaction parameter) describing interparticle interaction.

A semi-empirical relationship was proposed by Krieger and Dougherty [14] to include all particle volume concentrations. The equation describes the model:

$$\mu_{eff} = \mu_{bf}\left(1 - \frac{\emptyset}{\emptyset_m}\right)^{-[\eta]\emptyset_m} \tag{21}$$

For the above equation, $\emptyset_m$ is described as the maximum particle volume fraction at which flow can still occur. The intrinsic viscosity is 2.5 for monodispersed suspensions of hard spheres.

Other models based on Einstein's viscosity model are Lundgren [15], Graham [16], Saitô [17], Hatschek [18], Thomas and Muthukumur [19] and Frankel and Acrivos [20].

Meyer et al. [3] applied the Einstein model, as well as various other extend Einstein models, and found that each gave a different prediction.

Chen, Ding and Tan [21] noticed these widespread discrepancies and thus extended the experimental work of Krieger and Dougherty [14], leading to a new model. The model is based on the maximum packing fraction of agglomerates, as well as the fractal index of the agglomerates, leading to the equations:

$$\mu_{eff} = \mu_{bf}\left(1 - \frac{\emptyset_a}{\emptyset_m}\right)^{-[\eta]\emptyset_m} \tag{22}$$

$$\emptyset_a = \frac{\emptyset}{\emptyset_{ma}} = \emptyset\left(\frac{a_a}{a}\right)^{3-D} \tag{23}$$

where $\emptyset_{ma}$ is the packing fraction of the aggregates, D is the fractal index and $\frac{a_a}{a}$ is the ratio of the effective radii of the aggregates and primary nanoparticles.

New theoretical models

After the invention of nanofluids, new models had to be developed specifically for determining the viscosity of such nanofluids.

Based on their earlier work, Chen et al. [21] considered agglomeration as an important factor influencing viscosity, and proposed the following model:

$$\eta_r = \left(1 - \frac{\emptyset}{0.605}\left(\frac{a_a}{a}\right)^{1.2}\right)^{-1.5125} \tag{24}$$

Agglomeration, also known as aggregation, is the collection of mass or things. In this case, agglomeration is the collection of nanoparticles. When the nanoparticle form a collection it results in the formation of what can be seen as a larger particle. This particle now has a new effective radius/diameter which is larger than that of the original particles and which effects the composition of the nanofluid. As proven by Chen et al [21], the particle size directly affects the viscosity. Many other models also incorporate the particle size (diameter or radius) as a result of the effect that it has on the properties of the nanofluid, including viscosity.

Masoud Hosseini, Moghadassi and Henneke [22] produced a new dimensionless model to predict the viscosity of nanofluids. The equation describing the model is:

$$\mu_{nf} = \mu_{bf}.\exp\left[m + \alpha\left(\frac{T}{T_0}\right) + \omega(\emptyset_h) + \gamma\left(\frac{d_p}{1+r}\right)\right] \tag{25}$$

where $\emptyset_h$ is the hydrodynamic volume fraction of the nanoparticles, r the thickness of the capping layer and T_0 a reference temperature of 20 °C. The empirical constants α, ω and γ are obtained from experimental data.

Another model was proposed by Masoumi, Sohrabi and Behzadmehr [23]. This model showed acceptable agreement with experimental data. The model is defined by the equations:

$$V_B = \frac{1}{d_p}\sqrt{\frac{18K_BT}{\pi\rho_p d_p}} \tag{26}$$

$$\mu_{nf} = \mu_{bf} + \frac{\rho_p V_B d_p^2}{72C_1\delta} \tag{27}$$

$$\delta = \sqrt[3]{\frac{\pi}{6\emptyset}}\,d_p \tag{28}$$

$$C_1 = \mu_{bf}^{-1}\left[(c_1 d_p + c_2)\emptyset + (c_3 d_p + c_4)\right] \tag{29}$$

with c_1 to c_4 being obtained through experimental data.

Empirical models

Graf [24] was the first to recommend a specific form in which experimental results should be expressed, so as to allow comparison with theoretical models. The form in which the results are presented is given below:

$$\mu_{eff} = \mu_{bf}(1 + [\eta]\emptyset + [\eta]^2\emptyset^2 + [\eta]^3\emptyset^3 + [\eta]^4\emptyset^4 + \cdots) \tag{30}$$

The above empirical model for predicting the viscosity of nanofluids includes powers of ϕ, firstly showing that this expression is a functions of the volume fraction (ϕ). The powers are also an indication that the expression is a polynomial function which is valid over a specific range. The powers can also be seen as an indication of the shape of the graph that represents the model.

Avsec and Oblak [25] modified this expression, taking into consideration the nanolayer interaction effect. They presented the model:

$$\mu_{eff} = \mu_{bf}(1 + [\eta]\emptyset_{eff} + [\eta]^2{\emptyset_{eff}}^2 + [\eta]^3{\emptyset_{eff}}^3 + [\eta]^4{\emptyset_{eff}}^4 + \cdots) \quad (31)$$

with

$$\emptyset_{eff} = \emptyset\left(1 + \frac{h}{a}\right)^3 \quad (32)$$

where h is the thickness of the nanolayer and a is the particle radius.

Many models have been developed for specific nanofluids exposed to specific conditions. Many investigators observed through their experimental work that the effective viscosity of nanofluids is affected by the temperature of the medium, volume fraction, shear rate and size of the nanoparticles.

Each empirical model is for a specific nanofluid and is valid for a given volume fraction range, particle size and temperature range. The nanofluids for which empirical models are available contain nanoparticles of Al_2O_3, CuO, Cu, TiO_2, NiO, Ni, SiO_2, Fe_3O_4, Fe_2O_3 or Ag.

2.3.5.2 Thermal conductivity of nanofluids

To analyse the heat transfer of nanofluids, thermal conductivity is an important property that should be taken into account. Aybar, Sharifpur, Azizian, Mehrabi and Meyer [2] reviewed the various thermal conductivity models that are available.

Most models are based on the notion that diffusive heat transfer occurs in both the fluid and the solid phase. This notion would neglect the nanoscale effects that affect the properties of the nanofluid.

Different factors exist that could potentially influence the heat transfer enhancement of nanofluids. These factors are the Brownian motion of nanoparticles, clustering of nanoparticles, nanolayering of the liquid at the liquid/nanoparticle interface, ballistic transport and nonlocal effect, thermophoretic effect and near-field radiation. In the review, the models are categorised according to these factors, focusing on Brownian motion, nanolayering and clustering.

Brownian motions

In this case, there are two means that can affect the thermal conductivity. The first is when the particles transfer the heat themselves through their movement. The second is when micro-convection of the fluid around the nanoparticles takes place. The first effect was proven negligible and the second has been shown to have only a minor effect.

Several models have been developed. These models are summarised below.

Keblinski, Phillpot, Choi and Eastman [26] calculated thermal conductivity using the Green-Kubo relationship, which showed that the effect of the collisions between nanoparticles due to Brownian motions is not significant and that Brownian motion may have an effect in forming particle clusters. These clusters can then improve thermal conductivity.

Xuan, Li and Hu [27] offered a model taking into account the Brownian motion and the aggregation structure of nanoparticle clusters. Despite the model including Brownian motion effects, it cannot predict the linear relationship attached to the temperature. The proposed model is:

$$\frac{k_{eff}}{k_{bf}} = \frac{k_p + 2k_{bf} - 2\emptyset(k_{bf} - k_p)}{k_p + 2k_{bf} + \emptyset(k_{bf} - k_p)} + \frac{\rho_p \emptyset c_p}{2k_{bf}} \sqrt{\frac{K_B T}{3\pi\mu r_c}} \tag{33}$$

Das, Putra, Thiesen and Roetzel [28] explained that the major mechanism for thermal conductivity enhancement in nanofluids could be the stochastic motion of the particles. It was shown that, at low temperatures, the Brownian motion was unimportant to the conducting behaviour and that the stochastic motion of particles will be greater the smaller the particles.

Jang and Choi [29] constructed a model that consists of four modes of energy transport: collisions of the base fluid molecules, thermal diffusion in nanoparticle fluids, collisions between the nanoparticles due to the Brownian motion, and thermal interactions of dynamic nanoparticles with the base fluid molecules. The resultant model is:

$$k_{eff} = k_{bf}(1 - \emptyset_{eff}) + Bk_p\emptyset_{eff} + C_{pco}\frac{d_{bf}}{d_p} k_{bf} Re_{d_p}^2 \emptyset_{eff} \tag{34}$$

where B is a constant for the Kapitza resistance per unit area, C_{pco} is a proportional constant and the Reynolds number is calculated as:

$$Re_{d_p} = \frac{D_0 d_p}{l_{bf}\mu_{bf}} \tag{35}$$

with D_0 as the diffusion coefficient, and l_{bf} and μ_{bf} the liquid mean path and dynamic viscosity of the base fluid respectively.

Bhattacharya, Saha, Yadav, Phelan and Prasher [30] offered a model that was a linear combination of particle conductivity and fluid conductivity, where k_p is calculated by applying the Green-Kubo relation. The model is defined by:

$$k_{eff} = \emptyset k_p + (1 - \emptyset)k_{bf} \tag{36}$$

Kumar D, Patel, Kumar VR, Sundararajan, Radeep and Das [31] developed a hybrid model to take into account the large enhancement of the thermal conductivity of nanofluids based on the stationary and the moving particle model. The model employed the Stokes-Einstein formula for the

moving particle model. The kinetic theory of gases was also applied to obtain the effective thermal conductivity as:

$$\frac{k_{eff}}{k_{bf}} = 1 + C_{co}\bar{u}_p \frac{\emptyset r_{bf}}{k_{bf}(1-\emptyset)r_p} \tag{37}$$

where,

$$\bar{u}_p = \sqrt{\frac{2K_B T}{\pi \mu d_p^2}} \tag{38}$$

and C_{co} is a constant, K_B is the Boltzmann constant and r_p and d_p are the radius and diameter of the particle respectively. The model proposed by Kumar et al. [30] takes into account the thermal conductivity on particle size, volume fraction and temperature.

Koo and Kleinstreuer [32, 33] stated that the Brownian motion caused micro-mixing and is thus dominant in enhancing thermal conductivity. Their model, which takes into account temperature, particle size, volume fraction and the properties, is a combination of the static Wasp model and the dynamic model of thermal conductivity. The model contains terms representing the hydrodynamic interaction between particles and the augmented temperature dependence, which are difficult to obtain theoretically and should thus be determined experimentally.

Prasher, Bhattacharya and Phelan [34] modified the Maxwell-Garnett model to include Brownian motion. This led to a semi-empirical model for which the numerical simulation is needed to understand the exact origin of its empirical constraints.

An empirical correlation based on the Buckingham-Pi theorem was developed by Chon, Khim, Lee and Choi [35] for the thermal conductivity of nanofluids. The model is defined by the following equations:

$$\frac{k_{eff}}{k_{bf}} = 1 + 64.7\emptyset^{0.7460}\left(\frac{d_{bf}}{d_p}\right)^{0.3690}\left(\frac{k_p}{k_{bf}}\right)^{0.7476} Re^{1.2321}\,\mathrm{Pr}^{0.9955} \tag{39}$$

$$\mathrm{Pr} = \frac{\mu}{\rho_{bf}\alpha} \tag{40}$$

$$Re = \frac{\rho_{bf} u_p d_p}{\mu} \tag{41}$$

$$u_p = \frac{K_B T}{3\pi \mu d_p l_{bf}} \tag{42}$$

with a temperature-dependent expression being applied for the dynamic viscosity.

Ren, Xie and Cai [36] proposed a model based on kinetic theory-based micro-convection, liquid layering and conduction through both the particles and the fluid. A model was proposed by Jain,

Patel and Das [45], which took kinetic theory-based micro-convection, liquid layering and particle concentration into consideration.

Another semi-empirical model was developed by Prasher, Bhattacharya and Phelan [37], which showed that localised convection caused by Brownian motion is the main reason for enhancing thermal conductivity. This model combines the Maxwell model and convection caused by the particles in Brownian motion. It is called the multisphere Brownian model (MSBM) and is a modified version of the model developed by Prasher et al. [36].

The first fractal convection model was developed by Xu, You, Zhou and Xu [38] and took the fractal size distribution of the particles into account. The model showed good agreement with experimental data regarding the critical concentration for motion-induced convection.

Evans, Fish and Keblinski [39] developed a model that showed that the ratio of the thermal conductivity contribution caused by Brownian motion with respect to the thermal conductivity of the base fluid is proportional to the thermal diffusivity of the nanoparticle and base fluid. This led to their model:

$$\frac{k_{eff}}{k_{bf}} = 1 + 3\emptyset\,\frac{\gamma - 1}{\gamma + 2} \tag{43}$$

where γ is the ratio between the particle radius and the equivalent matrix thickness.

Vladkov and Barrat [40] modelled the thermal properties of nanofluids using molecular dynamics simulations, leading to the discovery that the Brownian motion of nanoparticles has no effect on the cooling process. This lead to their own model of thermal conductivity.

An analysis performed by Yu-Hua, Wei and Jian-Chao [41] included Brownian motion effect, particle agglomeration and viscosity temperature as influences on thermal conductivity. Their model combined the Maxwell model and Brownian effects based on Xuan et al. [27] and is defined as:

$$\frac{k_{eff}}{k_{bf}} = \frac{k_{p_{eff}} + 2k_{bf} - 2\emptyset_{eff}(k_{bf} - k_{p_{eff}})}{k_{p_{eff}} + 2k_{bf} - \emptyset_{eff}(k_{bf} - k_{p_{eff}})} + \frac{\rho_p \emptyset_{eff} c_p}{2k_{bf}}\sqrt{\frac{K_B T}{3\pi\mu r_c}} \tag{44}$$

where

$$\emptyset_{eff} = \left(1 + \frac{l_t}{r_p}\right)^3 \emptyset \tag{45}$$

$$l_t = \frac{1}{\sqrt{3}}\left(\frac{4\,m_{mw}}{\rho_{bf} N_A}\right) \tag{46}$$

with m_{mw} as the molecular weight of the liquid on the solid interface, and N_A being Avogadro's constant in the equation for the thickness of the liquid layer (l_t).

A microscopic model developed by Shukla and Dhir [42] predicts the thermal conductivity by dividing the net heat flux caused by Brownian motion into interaction parts neglecting the kinetic contribution.

Yang [43] developed a model to predict thermal conductivity that takes into account the heat transfer due to Brownian motion based on the kinetic theory of particles in the fluids under relaxation time approximations. The model is a combination of diffusive heat conduction and the particle Brownian motion. The model has the equation:

$$k_{eff} = \left(1 + 3\left(\frac{4}{3}\pi r_p^3\right)\frac{\frac{r_p}{R_b k_{bf}} - 1}{\frac{r_p}{R_b k_{bf}} + 2}\right)k_{bf} + 157.5\left(\frac{4}{3}\pi r_p^3\right)c_f u_p^2 \tau \tag{47}$$

with the particle relaxation time (τ) and the Brownian particle velocity (u_p) calculated as:

$$\tau = \frac{m_p}{6\pi\mu_{bf} r_p} \tag{48}$$

$$u_p = \sqrt{\frac{3K_B T}{m_p}} \tag{49}$$

Nie, Marlow and Hassan [44] derived an equation for the contribution of nanoparticle Brownian motion to the thermal conductivity of the nanofluid. Results showed that the thermal conductivity is proportional to the ratio of temperature (K) over viscosity. The equation is:

$$k_{excess} = \frac{85}{96\pi 2}\frac{\emptyset K_B^2 T}{r_p^4 \mu} \tag{50}$$

Vasu, Krishna and Kumar [45] derived equations to model the thermal conductivity of Cu-water and Al_2O_3-water nanofluids specifically. The model for Cu-water is:

$$\frac{k_{nf}}{k_{bf}} = 0.74\left(\frac{1}{\nu_p}\sqrt{\frac{18\,K_B T}{\pi\rho_p d_p}}\right)\emptyset^{0.05}\left(\frac{k_p}{k_{bf}}\right)^{0.2324} \tag{51}$$

while the model for Al_2O_3-water is given as:

$$\frac{k_{nf}}{k_{bf}} = \left(\frac{1}{\nu_p}\sqrt{\frac{18\,K_B T}{\pi\rho_p d_p}}\right)\emptyset^{0.05}\left(\frac{k_p}{k_{bf}}\right)^{0.2324} \tag{52}$$

Jain et al. [46] calculate the thermal conductivity for a specific case using the combined parallel model that implements the Brownian dynamic simulation technique and the Green-Kubo model. It was concluded that their model could properly predict the effective thermal conductivity of nanofluids in which the Brownian motion is the main mechanism for enhancement.

A model was predicted by Jung and Yoo [47], which implements the kinetic theory to determine thermal conductivity, while also considering the contribution of interparticle interaction due to the existence of the electrical double layer (EDL). The model is a modification of the Maxwell model and also accounts for temperature, particle size and volume fraction. The model had the form:

$$k_{eff} = K_{Maxwell} + k_{Brownian} + \left(1 + \frac{k_{EDL}}{k_{Brownian}}\right) \tag{53}$$

A combined static and dynamic model was developed by Murshed, Leong and Yang [48] that incorporates most of the possible parameters, including particle size, nanolayer, particle movements, interactions and the surface chemistry of the particles. The model is defined by the equation:

$$\begin{aligned} k_{eff-nf} &= \left\{ k_{bf} \frac{\emptyset_p \omega (k_p - \omega k_{bf}) \left[2\left(1+\frac{\delta_{nl}}{2r_p}\right)^3 - \left(1+\frac{\delta_{nl}}{r_p}\right)^3 + 1\right] + (k_p + 2\omega k_{bf})\left(1+\frac{\delta_{nl}}{2r_p}\right)^3 \left[\emptyset_p \left(1+\frac{\delta_{nl}}{r_p}\right)^3 - (\omega - 1) + 1\right]}{\left(1+\frac{\delta_{nl}}{2r_p}\right)^3 (k_p + 2\omega k_{bf}) - (k_p - \omega k_{bf})\emptyset_p \left[\left(1+\frac{\delta_{nl}}{2r_p}\right)^3 - \left(1+\frac{\delta_{nl}}{r_p}\right)^3 + 1\right]} \right\} \\ &+ \left\{ \emptyset_p^2 \left(1+\frac{\delta_{nl}}{2r_p}\right)^3 k_{bf} \left[3\left(\frac{k_{cp} - k_{bf}}{k_{cp} + 2k_{bf}}\right)^2 + \frac{3}{4}\left(\frac{k_{cp} - k_{bf}}{k_{cp} + 2k_{bf}}\right)^2 + \frac{9}{16}\left(\frac{k_{cp} - k_{bf}}{k_{cp} + 2k_{bf}}\right)^3 \left(\frac{k_{cp} + k_{bf}}{k_{cp} + 2k_{bf}}\right) + \frac{3}{2^6}\left(\frac{k_{cp} - k_{bf}}{k_{cp} + 2k_{bf}}\right)^4 \right. \right. \\ &\left. \left. + \cdots \right] \right\} + \left\{ \frac{1}{2}\rho_{cp} c_{cp} d_p \left[\sqrt{\frac{3K_B T \left[1 + 1.5\left(1+\frac{\delta_{nl}}{r_p}\right)^3 \emptyset_p\right]}{2\pi \rho_{cp} c_{cp} d_p \left(1+\frac{\delta_{nl}}{r_p}\right)^3 r_p^3}} + \frac{G_T}{6\pi\mu\left(1+\frac{\delta_{nl}}{r_p}\right) r_p d_p} \right] \right\} \end{aligned} \tag{54}$$

Xiao, Yang and Chen [49] proposed an analytical model that considered the effect of the convection between the particles and the liquid by taking the fractal distribution of the nanoparticles into account. The expression was given as a function of variables, including the properties of the base fluid and the nanoparticles.

Nanolayer

The next factor that influences the thermal conductivity is the nanolayer. Nanofluid structure consists of solid nanoparticles, solid-like liquid layers at the interface of the base fluid and nanoparticles, which are known as the nanolayers, and the base fluid [2].

Some models have been developed. These models are summarised below.

Yu and Choi [50] modified the Maxwell equation to include the effect of the nanolayer. For the modification, it was assumed that the nanolayer around each particle could be combined with the particle, forming an equivalent layer. Because the particle volume concentration was so small, it was assumed that no overlap of the equivalent particles would take place.

Feng, Yu, Xu and Zou [51] stated that the assumptions made by Yu and Choi [49] were not valid because the liquid molecules that surround the particle form part of an interfacial layer. The concentration of this interfacial layer is lower than that of the solid nanoparticle. This meant that the interfacial thermal conductivity should be higher than that of the fluid, but lower than that of the solid particle. Feng et al. [50] also estimated an upper limit for the thermal conductivity of the interfacial layer. The limit is described with the equations:

$$k_{eff} = \frac{k_{pe} + 2k_{bf} + 2(k_{pe} - k_{bf})\left(1 + \frac{\delta_{nl}}{r_p}\right)^3 \emptyset}{k_{pe} + 2k_{bf} - 2(k_{pe} - k_{bf})\left(1 + \frac{\delta_{nl}}{r_p}\right)^3 \emptyset} k_f \tag{55}$$

$$k_{pe} = \left[\frac{\left[2\left(1 - \frac{k_{nl}}{k_p}\right) + \left(1 + \frac{\delta_{nl}}{r_p}\right)^3 \left(1 + 2\frac{k_{nl}}{k_p}\right)\right]\frac{k_{nl}}{k_p}}{-\left(1 - \frac{k_{nl}}{k_p}\right) + \left(1 + \frac{\delta_{nl}}{r_p}\right)^3 \left(1 + 2\frac{k_{nl}}{k_p}\right)}\right] k_p \tag{56}$$

Yu and Choi [52] then modified the Maxwell model, which was limited to spherical particles. Next, they extended the Hamilton-Crosser model, which was valid for non-spherical particles, to include the nanolayer effect. The model includes parameters dependent on the particle sphericity or eccentricity.

Using non-equilibrium molecular dynamic simulations, the thermal resistance of the solid/liquid interface was calculated by imposing a temperature gradient. The simulations lead to the discovery of two distinct regimes of the Kapitza resistance.

Xue [53] presented a new model for effective thermal conductivity. The model is based on Maxwell's model and the average polarisation theory. This model was later proven by Yu and Choi [51] to overestimate thermal conductivity due to incorrect parameters.

From the general solution of the spherical-coordinate heat conduction equations, Xie, Fujii and Zhang [54] derived a new formula for the thermal conductivity of a nanolayer. The expression is given as:

$$k_{nl} = \frac{k_{bf}\left[\frac{k_p}{k_{bf}}\left(1 + \frac{\delta_{nl}}{r_p}\right) - 1\right]^2}{\left(\left[\frac{k_p}{k_{bf}}\left(1 + \frac{\delta_{nl}}{r_p}\right) - 1\right] - \frac{\delta_{nl}}{r_p}\right)\ln\left(1 + \left[\frac{k_p}{k_{bf}}\left(1 + \frac{\delta_{nl}}{r_p}\right) - 1\right]\right) + \frac{\delta_{nl}}{r_p}\left[\frac{k_p}{k_{bf}}\left(1 + \frac{\delta_{nl}}{r_p}\right) - 1\right]} \tag{57}$$

The above equation shows that the average thermal conductivity of a nanolayer is dependent on the thermal conductivity of the fluid, the reduced thermal conductivity of the nanoparticle, and the ratio of the nanolayer thickness to the original particle radius. The proposed expression for the thermal conductivity of the nanolayer was paired with a formula for effective thermal conductivity.

Based on Fourier's law, Leong, Yang and Murshed [55] proposed a model for effective thermal conductivity, which accounts for the effect of the interfacial layer. This model is defined as:

$$k_{eff} = \frac{(k_p - k_{nl})\emptyset_{nl}k_{nl}\left[2\left(1+\frac{\delta_{nl}}{2r_p}\right)^3 - \left(1+\frac{\delta_{nl}}{r_p}\right)^3 + 1\right] + (k_p + 2k_{nl})\left(1+\frac{\delta_{nl}}{2r_p}\right)^3\left[\emptyset_{nl}\left(1+\frac{\delta_{nl}}{r_p}\right)^3(k_{nl} - k_{bf}) + k_{bf}\right]}{\left(1+\frac{\delta_{nl}}{2r_p}\right)^3(k_p + 2k_{nl}) - (k_p - k_{nl})\emptyset_{nl}\left[\left(1+\frac{\delta_{nl}}{2r_p}\right)^3 + \left(1+\frac{\delta_{nl}}{r_p}\right)^3 - 1\right]} \tag{58}$$

with

$$\emptyset_{nl} = \emptyset_p\left[\left(1+\frac{\delta_{nl}}{r_p}\right)^3 - 1\right] \tag{59}$$

The model is limited by the fact that the thermal conductivity and thickness of the nanolayer had to be set to predict the experimental data. It is also assumed that the particles are far enough apart so as not to interact with each other.

Tillman and Hill [56] proposed a thermal conductivity profile for the nanolayer. This was a revised procedure used to determine the thickness of the nanolayer as well. The model suggests:

$$k_{nl}(r) = X(1 - Yr)^m \tag{60}$$

with X and Y being parameters that are determined from the continuity of thermal conductivity at the interface and m is a power law exponent.

Zhou and Gao [57] conducted an investigation into the effect of interfacial nanolayers on effective thermal conductivity and the mutual interaction of nearest-neighbouring inclusions. The proposed model is dependent on the volume fraction, thickness of the nanoshell, radius of the nanoparticles and thermal conductivity of the components.

Clustering

When using the two-step method to produce a nanofluid, clusters of nanoparticles can form. These clusters can be dispersed into individual nanoparticles, such as sonication. Publications exist on the effects of these treatments on the thermal conductivity of nanofluids.

Different researchers have experimentally observed different effects on the thermal conductivity with clustering. Wang, Zhou and Peng [58] observed that thermal conductivity is increased by the occurrence of clusters. In contrast, Karthikeyan, Philip and Raj [59] observed that thermal conductivity decreased with time due to clustering.

Wang et al. [58] explains the increase in thermal conductivity by stating that the cluster structures act as local percolation structures and thus add to enhancing the effective thermal conductivity of nanofluids. Similarly, Prasher, Bhattacharya and Phelan [34, 60] state that the thermal conductivity of nanofluids (purely based on conduction) can be enhanced by the aggregation of nanoparticles. This statement was proven using the effective medium theory and can be explained using aggregation kinetics.

To explain the decrease in thermal conductivity, it is stated that, in an area with a low nanoparticle density, the thermal conductivity is lower as the base fluid has a lower thermal conductivity. When clustering occurs, settling is more likely to ensue, leading to a lower concentration of nanoparticles in the fluid itself. This would reduce the effective thermal conductivity, as particle-free zones are being created.

Hybrid models

Hybrid models are needed to take into account all possible mechanisms affecting the thermal conductivity of nanofluids. Very few hybrid models have been reported, with only a few worth mentioning.

These include the combination models proposed by Murshed et al. [48] and Avsec [61].

Corcione [62, 63] proposed an empirical relation based on experimental data. The relation is given as:

$$\frac{k_{eff}}{k_{bf}} = 1 + 4.4Re^{0.4}\,\mathrm{Pr}^{0.66}\,\emptyset^{0.66}\left(\frac{T}{T_{fr}}\right)^{10}\left(\frac{k_p}{k_{bf}}\right)^{0.03} \tag{61}$$

with

$$Re = \frac{2\rho_{bf}K_BT}{\pi\mu_{bf}^2 d_p} \tag{62}$$

Taking the effects of the nanoscale, the interfacial interaction between the nanoparticles and the liquid molecules and Brownian motion into account, Xuan et al. [26] derived the following model:

$$k_{eff} = \frac{k_{pn} + 2k_{bf} - 2\emptyset_{eff}(k_{bf} - k_{pn})}{k_{pn} + 2k_{bf} + \emptyset_{eff}(k_{bf} - k_{pn})}k_{bf} + \frac{\rho\emptyset_{eff}c_p}{2}\sqrt{\frac{k_BT}{3\pi r_c\mu_{nf}}} \tag{63}$$

Nabi and Shirani [64] introduced a theoretical hybrid model based on the Maxwell model. This model takes Brownian motion into account, as well as the resulting micro-mixing of nanoparticles and clusters, the aggregation kinetics of nanoparticles and clusters.

Other effects

Other mechanisms that affect thermal conductivity that have not been discussed include particle settling down time, temperature, pH, dispersion and the particle size effect on the surface contact of the liquid/particle interaction.

2.3.5.3 Other thermophysical properties

Different methods and models also exist to predict the thermal expansion coefficient, density and specific heat capacity of nanofluids. In most cases, these thermophysical properties are determined by the following equation, as given by Ho, Liu, Chang and Lin [65]:

Density:

$$\rho_{nf} = \varphi_{nf}\rho_p + (1 - \varphi_{nf})\rho_{bf} \tag{64}$$

Thermal expansion coefficient:

$$\rho_{nf}\beta_{nf} = \varphi_{nf}\rho_p\beta_p + (1 - \varphi_{nf})\rho_{bf}\beta_{bf} \tag{65}$$

Specific heat capacity:

$$\rho_{nf}\, C_{p,nf} = \varphi_{nf}\, \rho_p C_{p,p} + (1 - \varphi_{nf})\rho_{bf} C_{p,bf} \tag{66}$$

A recent paper published by Sharifpur, Yousefi and Meyer [66] proved that the density of a nanofluid is affected by the nanolayer (which is, in turn, affected by the particle size, and then the material). Due to this discovery, the density of a nanofluid can be determined using the following equation:

$$\rho_{nf} = \frac{\varphi_{nf}\rho_p + (1 - \varphi_{nf})\rho_{bf}}{(1 - \varphi_{nf}) + \frac{\varphi_{nf}(r_p + t_v)^3}{{r_p}^3}} \tag{67}$$

where,

$$t_v = -0.0002833{r_p}^2 + 0.0475r_p - 0.1417 \tag{68}$$

The thermophysical properties of a nanofluid can, however, be determined experimentally.

Depending on the specific nanofluid and the conditions that it is exposed to, a model can be chosen from the various developed models that are available. Alternatively the properties can be determined experimentally using specialised equipment.

2.4 Previous works

To better understand the field of nanofluids, a detailed literature review is done on past works. For this section of the literature study, two categories are considered: experimental work and numerical work.

2.4.1 Previous experimental works

For this section, publications on experimental work done on heat transfer through natural convection in a cavity filled with a nanofluid are investigated.

Ho, Chen, Yan and Mahian [67] performed an experimental investigation into natural convection heat transfer of Al_2O_3-water nanofluids within a rectangular cavity (25 mm x 25 mm x 60 mm) where the top wall was kept at a higher temperature than the bottom wall, while the side walls were thermally insulated. For the experiments, nanofluids with volume fractions of 1%, 2%, 3% and 4% were prepared and tested. A numerical study was also performed. The comparison of the experimental and numerical data showed that the Nusselt numbers of both studies were similar when the Ludwig-Soret effect, Brownian motion and sedimentation of the particles are accounted for within the numerical model.

Experiments were performed by Chein and Chuang [68] to study micro-channel heat sink performance using nanofluids as coolants. As a nanofluid, CuO particles were suspended within water with a volume fraction range of 0.2% to 0.4%. It was discovered that, for high flow rates, the heat transfer was dominated by the volume flow rate and that the nanoparticles had no effect. Slight pressure drops due to the presence of nanoparticles were observed.

The heat transfer characteristic of diluted nanofluids was experimentally studied by Rao and Srivastava [69]. They tested for buoyancy-driven convection in a heated cavity containing Al_2O_3-water diluted nanofluids at volume concentrations of 0.01%, 0.02%, 0.03% or 0.04%. For the base fluid (deionised water) tests, it was discovered that conduction took place predominately, while for the nanofluids, heat transfer took place via convection. The results showed that the heat transfer coefficient increased with an increase in the temperature difference, as well as an increase in the percentage of the volume concentration.

A previous study by Rao and Srivastava [70] involved heat transfer between a vertical heated flat plate and an Al_2O_3 nanofluid. Volume fractions in the range of 0.005% to 0.02% were tested and the heat transfer mapped using laser interferometry. Compared to the base fluid, an enhancement of 21% was noticed in the heat transfer coefficient for a concentration of 0.02%.

Afifah, Syahrullail and Azwadi [71] presented results from their experimental study of an Al_2O_3-water nanofluid in a square cavity heated at the bottom. The investigation into the heat transfer through natural convection was done for various volume fractions within the range of 0% to 2% and different heating times varying between 0 and 35 minutes. Different dispersing techniques were also investigated, leading to findings that indicate that the viscosity of the nanofluid is dependent on the technique used. It was concluded that transport mechanism, thermophoresis and Brownian motion have an effect on the heat transfer.

Putra, Roetzel and Das [72] performed experiments to analyse heat transfer occurring through the natural convection of nanofluids in a horizontal cylinder heated from one end and cooled from the other. Nanofluids were tested that had been produced with CuO and Al_2O_3 particles respectively, suspended in water with volume fractions of 1% and 4% each. It was found that the thermal conductivity enhancement was directly related to the temperature, with the highest thermal conductivity enhancement occurring with the 4% CuO nanofluid.

From the results, it is clear that the thermal conductivity was enhanced by the nanoparticles. It was also found that the CuO nanofluids show more enhancement than the Al_2O_3 nanofluids.

Experiments conducted by Jahanshahi, Hosseinizadeh, Alipanah, Dehghani and Vakilinejad [73] with a SiO_2-water nanofluid were done to investigate the heat transfer enhancement. The experiments were performed within the volume fraction range of 0% to 4% and Rayleigh number range of $10^5 < Ra_f < 10^7$ in a square cavity with different side wall temperatures. It was observed that the Nusselt number increases with volume fraction for the entire Rayleigh number range.

Heris, Pour, Mahian and Wongwises [74] produced a comparative experimental study on natural convection heat transfer for different nanoparticles. The nanopowders Al_2O_3, TiO_2 and CuO were all suspended in turbine oil as 0.2%, 0.5% and 0.8% weight fractions. The experiment was not only designed to compare the different nanofluids, but also to investigate the effects of inclination angle on the natural convection in the cubic cavity (10 cm x 10 cm x 10 cm).

The experiments were done for inclination angles (with respect to the horizontal one) of 0°, 45° and 90°. The results showed that, for all inclination angles, the base fluid had the highest Nusselt number, while for the nanofluids with 0.8% weight fraction, CuO had the highest Nusselt number.

The table below summarises the details on the investigations in the same order as discussed above.

Table 1: Summary of past experimental works

		Range				Model		Cavity		
Author	**Nanofluid**	**Volume fraction (%)**	**Rayleigh number**	**Temperature (°C)**	**average particle size (nm)**	**thermal conductivity**	**viscosity**	**type**	**dimensions (mm)**	**Comments**
Ho et al.	Al_2O_3/water	1, 2, 3 & 4	$5.78x10^5$ - $3.11x10^6$	19.9-30.1	33	measured experimentally		rectangular	25x25x60	
Chein and Chuang	Cuo-H_2O	0.2 - 0.4			80x20	measured using KH2 thermal property meter	Brinkman	microchannel heat sink		heat source (25.3W)
Rao and Srivastava	Al_2O_3/water (deionized)	0.01, 0.02, 0.03 & 0.04	$3.7x10^5$ - $5x10^4$	ΔT = 1 to 2.3°C	13	experimental correltation by Sharma et al.		rectangular	25x20x60	
Rao and Srivastava	Al_2O_3/water	0 - 0.02		ΔT = 1.2°C	13	measured experimentally		vertical heated flat plate immersed in nanofluid	30x75	
Afifah et al.	Al_2O_3/water	0 - 2	NA		30	measured experimentally		square (heated at bottom)		comparing different preparation methods, heating time varied (0 to 35min)
Putra et al.	Al_2O_3 and CuO in water	0, 1 & 4	$16x10^6$ - $92x10^6$	20 - 75	Al_2O_3 - 131.2; CuO - 87.3	Das et al.	measured by a disc type rotating rheometer	horizontal cylinder	L/D = 0.5; L/D = 1	heated from one end and cooled form the other
Jahanshahi et al.	SiO_2/water	0 - 4	10^5 - 10^7		12	Abu-Nada and measured experimentally	Ho et al.	square		
Heris et al.	Al_2O_3, TiO_2 and CuO in turbine oil	0.2, 0.5 & 0.8 (weight fraction)	$3x10^7$ - $3x10^8$		Al_2O_3 - 20; TiO_2 - 20; CuO - 60	Hamilton-Crosser	Brinkman	cubic	100	heating element (max 1000W), inclinde angles of 0°, 45° & 90°

2.4.2 Previous numerical works

For this section, publications on CFD work on heat transfer through natural convection in a cavity filled with a nanofluid are investigated.

The field of CFD does not only include commercial CFD software, but also open-source programmes and self-coded programmes. Most available investigations are focused on forced convection, with only few in the field of natural convection.

Commercial CFD software includes packages such as ANSYS-FLUENT and FloEFD. Not many studies have been performed using such software. Yu, Wang, Zu, Fan, Hu and Cen [75] conducted a

numerical study in ANSYS- FLUENT in conjunction with the SIMPLE algorithm for a transient natural convection case in a differentially heated square cavity filled with CuO-water nanofluid.

Ternik [76] performed an investigation into the heat transfer through steady-state natural convection in a cubic enclosure using the open-source software OpenFoam. The investigation was conducted for water-Au nanofluid and the programme was written in C++.

The Lattice-Boltzmann method is a technique that can be used to model fluid problems. This technique has been employed by several researchers to analyse the natural convection heat transfer of nanofluid in a cavity. Among others, He, Qi, Hu, Qin, Li and Ding [77] implemented this method to analyse natural convection in alumina-water nanofluids, Fattahi, Farhadi, Sedighi and Nemati [78] used the Lattice-Boltzmann method to analyse both Al_2O_3 and CuO nanofluids and Sajjadi, Gorji, Kefayati and Ganji [79] used a Lattice-Boltzmann simulation to analyse natural convection in a tall cavity filled with Cu-water nanofluid.

The SIMPLE algorithm is a numerical procedure that is widely used to solve the Navier-Stokes equations, which is the goal in CFD. The algorithm is used to solve any model that is chosen to describe the convection. Corcione, Cianfrini and Quintino [80] solved the two-phase mixture model using the SIMPLE algorithm, while Alinia, Gorji-Bandpy, Ganji, Soleimani, Ghasemi and Darvan [81] also chose to solve the two-phase mixture model using the algorithm. More publications on the implementation of the SIMPLE algorithm to analyse natural convection include Abouali and Falahatpisheh [82], Sheikhzadeh, Dastmalchi and Khorasanizadeh [83] and Cianfrini, Corcione, Habib and Quintino [84].

When a nanofluid is modelled numerically, two main methods exist: the nanofluid can either be modelled as a single-phase fluid or as a two-phase fluid.

If the nanofluid is modelled as a single-phase fluid, it is assumed that it can be represented as a fluid with altered thermophysical properties. Using a single-phase model simplifies the application of CFD. This is because only the fluid properties and the governing equations have to be modified. Single-phase models are also called homogenous models.

Two-phase models are based on the assumption that the base fluid and the nanoparticles are modelled separately. Two-phase models are also called heterogeneous, non-homogenous or transport models. Two-phase models are more complex than single-phase models.

The table below summarises which of the abovementioned numerical investigations selected single-phase and which selected two-phase models.

Table 2: Single- and two-phase numerical investigations

Single-phase	**Two-phase**
Yu et al. [75]	He et al. [77]
Ternik [76]	Fattahi et al. [78]
Sajjadi et al. [79]	Corcione et al. [80]
Cianfrini et al. [84]	Alinia et al. [81]
	Abouali and Falahatpisheh [82]
Sheikhzadeh et al. [83]	

From Table 2, it can be seen that both single-phase and two-phase models are regularly used. One comparative investigation was found by Sheikhzadeh et al. [83], where it is concluded that even though the two-phase model is more accurate, it is computationally more expensive. Due to the conclusion, the phase model to be used depends on the application.

Other methods to analyse heat transfer due to natural convection also exist. Researchers can use other techniques to code their own programmes using software such as MATLAB or PYTHON to implement them.

For most numerical studies, a method of validation is needed. This can be done by comparing the results obtained from the numerical study with the experimental results.

2.5 Past research into TiO_2 water-based nanofluids

After the nanofluid TiO_2 in a water base was selected as the nanofluid that would be investigated, a detailed investigation was done into previous works in this field. Focus was placed on natural convection heat transfer in an enclosure.

Moradi, Bazooyar, Eternad and Moheb [85] investigated the influence of the geometry of a cylindrical enclosure on the heat transfer of Ti and Al_2O_3 nanofluids. The lower surface of the enclosure has a constant heat flux and was investigated experimentally. It was found that for the TiO_2 nanofluid, the heat transfer coefficient was lower than that of the base fluid under the same conditions.

Hu, He, Wang, Wang Q and Schlaberg [86] meanwhile performed an experimental and numerical investigation into the heat transfer of a TiO_2-water nanofluid with mass fractions of 3.85%, 7.41% and 10.71% in a square enclosure. The numerical aspect of the investigation involved a Lattice-Boltzmann model coupling transfer. Good comparison was found between the numerical and experimental results, while no improvement was found in the heat transfer of the nanofluid in comparison to that of the base fluid.

A study performed by Ganji and Malvandi [87] added the aspect of a uniform magnetic field. The theoretical study investigated water-based Ti and Al nanofluids in a vertical enclosure. This study observed that the particles within the fluid tend to migrate from the heated walls towards the cold walls, creating a non-uniform distribution of nanoparticles.

Another numerical study based on the Lattice-Boltzmann model was done by Sheikholeslami, Ashorynejad and Rana [88]. The investigation simulated the nanofluid flow and heat transfer of alumina-, Cu-, titania- and Ag-water-based nanofluids inside a square enclosure containing a rectangular heated body. The Brinkmann model was used to calculate the effective viscosity, while the thermal conductivity was determined using the Maxwell-Garnett model. It was discovered that the effect of the nanoparticle volume fraction is more noticeable for low Rayleigh numbers.

Ouyahia, Benkahla and Labsi [89] numerically investigated the hydrodynamic and thermal properties of a TiO_2-water nanofluid in a cavity with a triangular cross-section. The base wall was kept at a high temperature, while the other two walls had a constant cold temperature for the study. The SIMPLER algorithm was used to solve for the fluid flow and the heat transfer. It was found that the heat transfer was enhanced, with the effect being more evident in the case of a higher Rayleigh number.

The study also investigated the inclination angle and found that it affected the heat transfer significantly.

From investigation into past research into water-based TiO_2 nanofluids, it is clear that little research has been conducted to date.

2.6 Background of the methods used in experimental studies

To perform an experimental investigation, certain equipment is needed to complete the experiments. This section briefly discusses the necessary equipment for both the preparation of the nanofluids and the testing of the natural convection of a nanofluid in a cavity. The information in this section summarises what the student has discerned from other experimental investigations.

2.6.1 Preparation of the nanofluid

As the two-step method is commonly used, equipment needed for this method will be mentioned and discussed.

2.6.1.1 Weight balance

A scale is needed to accurately measure the amount of base fluid and nanoparticles needed to achieve a certain volume fraction. The volume fraction is calculated using the equation:

$$\emptyset = \frac{V_{np}}{V_{nf}} \tag{69}$$

Using density, the volume can be related to the mass, which can be measured on the scale.

2.6.1.2 Ultrasonicator

Once the nanoparticles have been dispersed into the base fluid, the newly formed nanofluid must be treated to ensure homogenous dispersion of the particles. A method of ensuring homogenous dispersion is to treat the fluid using ultrasonic waves. These waves, created by the ultrasonication tip that is placed into the fluid, cause any clusters in the nanofluid to disperse.

2.6.2 Current experimental setup

To investigate the heat transfer in a cavity filled with a nanofluid, a specific experimental setup is needed. The experimental setup is made up of the following elements:

2.6.2.1 Cavity

As the experiment aims to investigate natural convection inside a cavity, a cavity is needed. This cavity should have precise dimensions (which are known) and is mainly manufactured from an

insulating material. The only walls of the enclosure that are not manufactured with this insulating material are the opposite vertical walls, which are to be heated and cooled.

2.6.2.2 Heat exchangers

As walls with a constant temperature are impossible to achieve in an experimental investigation, shell-and-tube heat exchangers can be used to emulate the constant wall temperature effect. A unique shell-and-tube heat exchanger design manufactured from copper can be used to achieve this effect.

2.6.2.3 Thermal baths

The heat exchangers that emulate the constant wall temperatures utilize heated and cooled refrigerants, such as water, to create the temperatures. The specific water temperatures are achieved with the help of thermal baths, which can be set to specific temperatures.

2.6.2.4 Flow meters

To calculate the heat transferred by each heat exchanger, the flow rate of the water flowing through the tube and the shell is needed. Flow meters positioned on the inlet and outlet pipes can be used to provide the volume flow rate. This, in turn, can be used to calculate the mass flow rate.

2.6.2.5 Thermocouples

Temperature measurements at the inlets and outlets of the heat exchangers are necessary to determine heat transfer. Using thermocouples that are precisely placed in the centre of the tubes, the temperature measurements can be taken. More thermocouples are placed inside the walls of the heat exchangers to allow the precise measurement of the temperatures of the wall. Thermocouples can also be placed inside the cavity, submerged in the fluid, to model the flow within the cavity.

2.6.2.6 Data acquisitioning system

A data acquisitioning system is needed to record all measured data. This data is stored and later analysed.

Other equipment, such as beakers, personal protective equipment and storage containers – although essential – is not discussed in this section.

2.6.3 Safety and personal protective equipment

As nanofluids are a relatively new field, the dangers and possible safety hazards of working with these particles are mainly unknown. This calls for extra caution when dealing with the nanoparticles or nanofluids.

Personal protective equipment in the form of gloves, safety glasses, a gas mask and a lab coat should be worn during testing, and special care should be taken to regularly wash your hands, especially

after preparing the nanofluid or performing experiments. Furthermore, as ultrasonication is a noisy process, hearing protecting should be worn when the equipment is switched on.

2.7 Proposed investigation

After performing a detailed literature study into nanofluids and the work that has already been conducted in this field, the study was focused on TiO_2-deionised water nanofluids. From this investigation, it was found that very little work has been done in this field. Due to this, the focus of the investigation was obtained:

An experimental and numerical investigation into the natural convection heat transfer capacity of TiO_2 nanofluids (with deionised water as a base fluid) in a rectangular cavity with two constantly heated opposing walls. The volume fraction range to be investigated would be between 0% and 0.8%, while ranging the temperature difference between the two opposing walls between 20 °C and 50 °C. The properties of the fluid would be determined experimentally or by using a mathematical model, and the numerical study would be done using CFD software.

2.8 Summary

A detailed literature study was completed on nanofluids and natural convection. The available models to predict the thermal conductivity and viscosity of nanofluids were cited. The past works, numerical and experimental, on nanofluids were summarised in detail and discussed.

The literature study revealed many available models for the prediction of the thermal conductivity and viscosity of nanofluids. Some of the models are specific to a nanofluid, while others describe the general properties of nanofluids.

The investigation into past works on natural convection in nanofluids in a cavity resulted in the study of many publications on numerical studies. Different methods had been employed to solve the problem using either the single-phase or the two-phase mixing model. Very few experimental studies were found, reinforcing the need for further experimental investigations. This need is further emphasised by the contradictory results on enhancing heat transfer obtained from the available works. Experimental results are vital, as these are needed in the validation process of numerical works.

Very few investigations have been conducted in the field of the natural convection heat transfer of TiO_2 nanofluids. Due to this, it was decided to focus this investigation on this area, specifically using the case of a nanofluid in a square cavity with opposing walls of a constant temperature. This case would be investigated experimentally and numerically.

3. Experimental investigation

3.1 Introduction to the experimental investigation

Particles of TiO_2 are suspended in deionised water through sonication and pH-level adjustment with the hope of increasing the heat transfer capabilities of the base fluid. The properties of this nanofluid are investigated and modelled in an attempt to characterize the fluid. To investigate heat transfer through this nanofluid, an experiment is designed that involves heat exchangers and a square cavity.

3.2 Safety of the experimental investigation

As nanofluids are a relatively emerging field, with many gaps still to be filled with research, the safety of using these fluids is still unknown.

In order to ensure the safety of the person performing the experiment, safety measures are introduced. The student used the following personal protective equipment:

- Chemical-resistant gloves
- Lab coat
- Safety glasses
- Respiratory mask

Additional measures are taken to limit the possibility of exposure to the nanoparticles:

- The used nanofluid is disposed of safely as chemical waste.
- The working area is kept clean and well ventilated.

3.3 Nanofluid preparation

The nanofluid is sourced from the US Research Nanomaterials Inc. as a concentrate of titanium dioxide particles dispersed in deionised water to a weight percentage of 15wt%. The nanofluid is then prepared by diluting the TiO2-water concentrate with deionised water, creating 1.2 litres of a mixture with a specific volume fraction. Using an electronic scale, the exact amount is weighed to an accuracy of ±0.005 g. The nanofluid and water are then mixed in a 2-litre glass beaker. This mixture is sonicated for three minutes using the Hielscher UP200S ultrasonic processor with 0.7 cycle time and 80% amplitude. During the sonication process, the glass beaker in which the fluid is held is kept in a thermal bath set to a temperature of 15 °C to avoid evaporation of the nanofluid. The temperature and sonication time are kept low to ensure that the particles are not burnt, while still achieving the suspension of the particles in the fluid and avoiding clustering. To ensure that the nanofluid is sufficiently stable, the pH of the fluid is adjusted. A diluted base of sodium hydroxide (NaOH) and a dilute acid of hydrogen chloride (HCl) are used to achieve a pH value of 9.5.

3.4 Stability of the nanofluid

Before a nanofluid can be researched in detail, it is important to investigate the stability of the fluid. A stable fluid is one where the particles that were introduced remain suspended in the fluid and do not settle at the bottom. No separating occurs.

There are different methods to investigate the stability. The stability of the nanofluid is tested by means of two tests: visual and chemical.

3.4.1 Visual stability of the nanofluid

When analysing visual stability, a small sample of the nanofluid is prepared and placed in a glass or plastic container so that the fluid is visible. The container is placed in front of a plain background (black, blue or white) and a photograph is taken. More photographs are taken at later stages (hours, days or weeks later). The different photographs are then compared, checking for sedimentation in the later pictures and comparing the colour of the fluid.

If no sedimentation takes place, and the colour and composition appear constant over a certain time period, the fluid is said to be visually stable over this period.

3.4.2 Chemical stability of the nanofluid

Different methods exist to check chemical stability. These methods use the absorptivity and the zeta potential of the fluid.

3.4.2.1 Absorptivity

The absorptivity of a fluid is measured using a spectrophotometer. After preparing the nanofluid, it is placed in a tube, which is then placed on a slot in the spectrophotometer. As the base fluid is deionised water, a sample of deionised water is placed in the machine as a baseline for the measurement.

The absorptivity is tested over a wavelength range of 200 to 900 µm. The peak absorptivity and the wavelength at which it occurs are recorded. Over a period of time, the absorptivity at this wavelength is recorded at set time intervals. If the absorptivity remains stable over this period, the nanofluid is said to be chemically stable (absorptive) over this period of time.

3.4.2.2 Zeta potential

The nanofluid's chemical stability can also be tested by measuring its zeta potential. The fluid is placed in a special cell that is then placed in the Zetasizer Nano Series (last calibration date eight months before the tests were completed is sufficient), which can measure zeta potential, as well as size. A graph is produced that shows the distribution of the zeta potential as opposed to the amount. The zeta potential at the peak is taken as the zeta potential of the nanofluid. According to convention, the zeta potential value gives an indication of the stability of the fluid. If the zeta potential of the nanofluid is above 30 mV, the fluid can be assumed to be stable.

Due to the milky colour of the TiO_2 nanofluid, both methods used to test the chemical stability are limited. The zeta potential method and the absorptivity method can only be used at maximum volume fractions of 0.001%. This value is much lower than the minimum volume fraction intended for this set of experiments, which is 0.05%.

Because of the limitations of the chemical stability tests, it was assumed that if the low volume fractions are stable, the higher volume fractions are also stable. Visual stability experiments were performed to confirm this assumption.

Figure 1 below shows a sample of the nanofluid (volume fraction 0.4%) shortly after preparation (left) and 30 days later (right). These samples represent an intermediate volume fraction from the overall investigation.

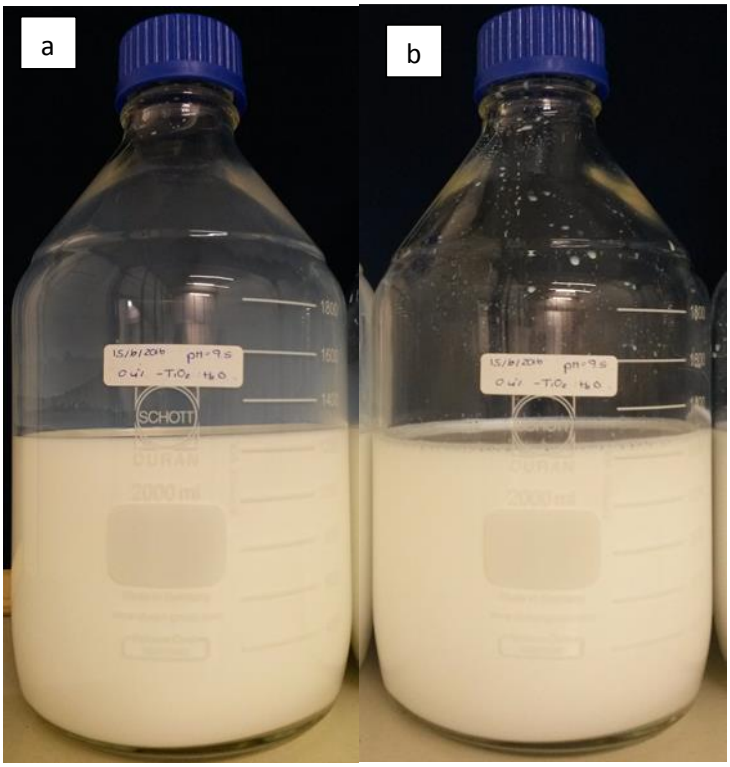

Figure 1: Visual stability check over 30 days: a) immediately after preparation; and b) 30 days after preparation

It can clearly be seen that over an extended period of time, the colour and consistency remain visually constant. Due to this observation, it can be stated that, over this period of time (30 days), the nanofluid sample is stable. The same visual inspection was done for a sample of each of the volume fractions involved in this investigation.

The reason that stability is needed is because without it, there would not exist a nanofluid but rather a fluid with particles in it. If the fluid is not stable, then the particles have not bonded with the fluid and the van der Waals forces between the particles are still in play, allowing for sedimentation and/or clustering to occur. By adjusting the pH-level of the nanofluid, ultrasonication of the fluid or by the addition of a binding agent, the likelihood of stability can be increase as the van der Waals attractive forces are reduced. There is currently however, no guarantee for stability.

3.5 Properties of the nanofluid

A fluid is defined by its physical and thermophysical properties. To accurately define the nanofluid consisting of TiO_2 particles and deionised water as a base fluid, the fluid's thermal conductivity, density, dynamic viscosity, specific heat capacity and thermal expansion coefficient are required.

To define the properties of the nanofluid, the properties of the nanoparticles (TiO_2) and the base fluid (deionised water) used to prepare the nanofluid are required.

3.5.1 Properties of the nanoparticles and the base fluid

For the experimental investigation, a concentrated (15 wt%) deionised water-based TiO_2 was purchased from US Research Nanomaterials Inc. The supplier specified that the TiO_2 particles had an average particle diameter of 5 to 15 nm. To confirm the size, a transmission electron microscopy (TEM) image of a sample of the fluid was requested from the Council of Scientific and Industrial Research (CSIR). The figures below show the TEM image:

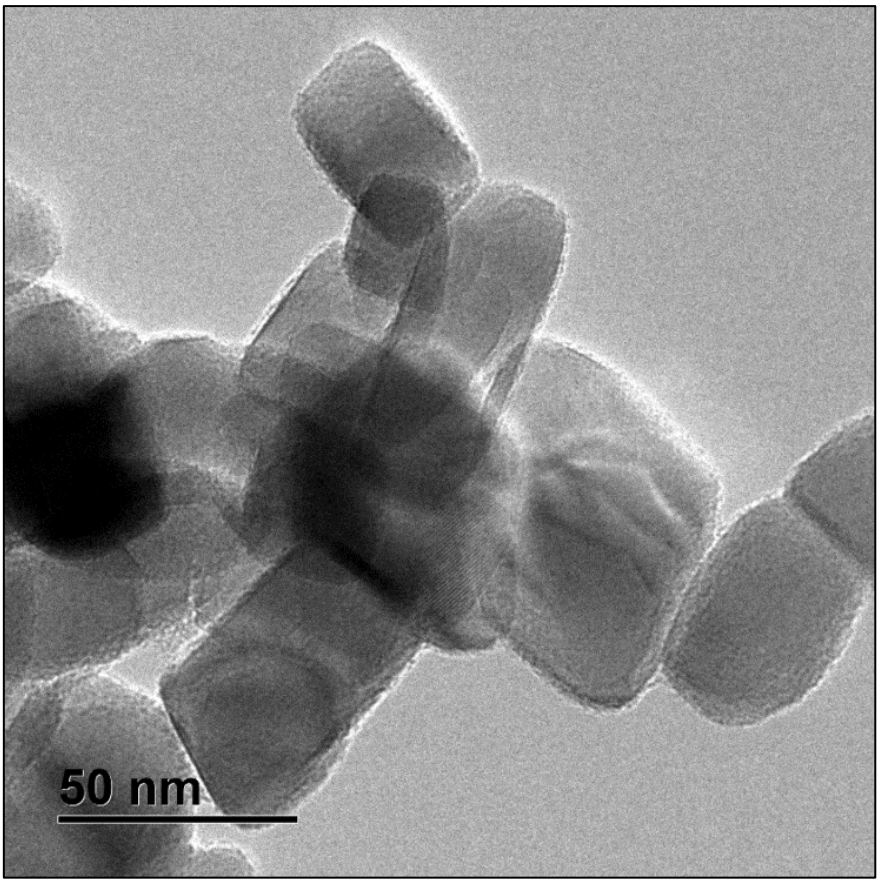

Figure 2: TEM of the concentrated nanofluid (50 nm)

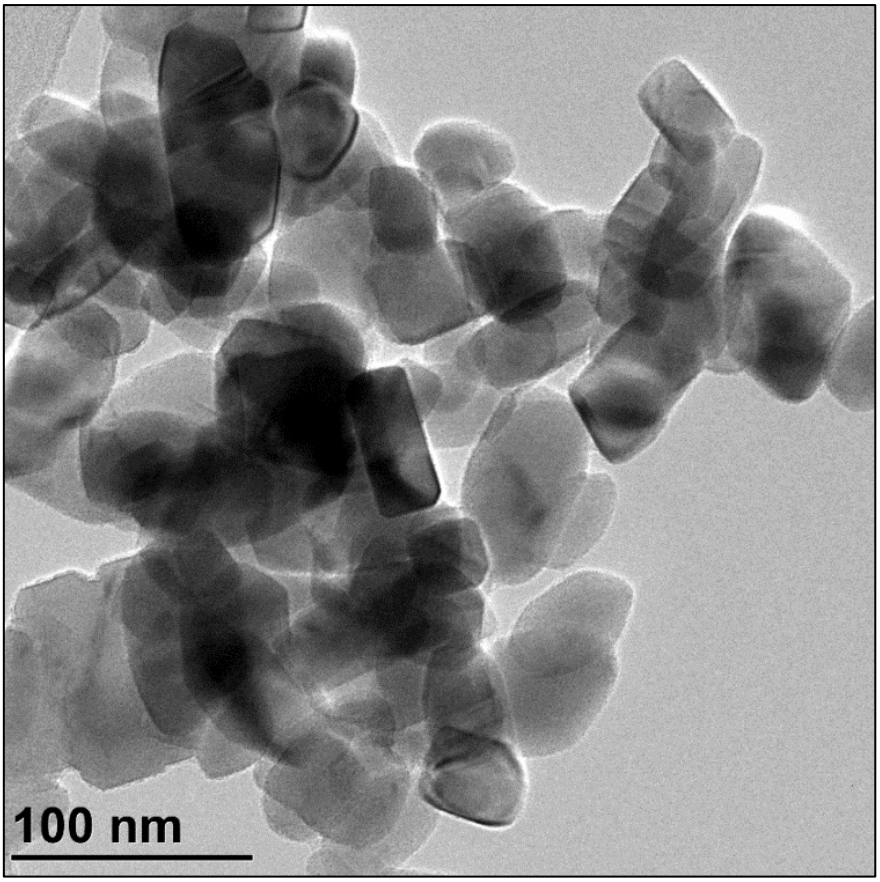

Figure 3: TEM of the concentrated nanofluid (100 nm)

From the above figures, it was determined that the average particle diameter was 50 nm.

Using the TEM image taken of the nanofluid and the scale given on the image (as seen below), the average particle diameter was determined as follows:

Using the scale, the approximate length and width (as they are more rectangular shaped than spherical), the average (add length and width and divide by 2) was determined. The average of all the particles was taken.

From this the standard deviation (σ) was calculated using the equation:

$$\sigma = \sqrt{\frac{1}{N}\sum_{i=1}^{N}(x_i - \mu)^2} \tag{70}$$

Where N is number of data points 100) and μ is the mean (50nm) of the data. This results in a standard deviation of 10.8.

Due to the costs involved in producing a TEM image, the images used in the determination of the average particle size were limited.

To ensure that the nanofluid is homogenous (as much as possible) throughout, the mixture is ultrasonicated. This means that sound energy (in the ultra-frequency range) is applied to agitate the

samples and distribute them evenly. As the entire nanofluid was ultrasonicated, the fluid is considered homogenous throughout. This would result in the same average particle size regardless of the sample that is tested.

Table 3 below shows the properties of the base fluid, deionised water, and nanoparticles, TiO_2, at an average temperature of 30 °C.

Table 3: Properties of the nanoparticles and the base fluid

Property	Unit	Deionised water	Titanium dioxide
Density	kg/m^3	996	4 250
Specific heat capacity	J/kgK	4 178	686
Thermal conductivity	W/mK	0.615	8.9538
Dynamic viscosity	kg/ms	0.0008	-
Thermal expansion coefficient	1/K	0.00021	1.7 E-07
Particle size	nm	-	50

When determining the properties of the nanofluid, the temperature and volume fraction are to be taken into account.

3.5.2 Thermal conductivity of the TiO_2 nanofluid

Different models exist that can be used to estimate the thermal conductivity of a nanofluid. The following models were compared:

Buongiorno [90]:

$$k = k_{bf}\,(1 + 1.292\emptyset - 11.99\emptyset^2) \tag{71}$$

Maxwell-Garnett [91]:

$$\frac{k_{nf}}{k_f} = \frac{k_s + 2k_f - 2\emptyset(k_f - k_s)}{k_s + 2k_f + \emptyset(k_f - k_s)} \tag{702}$$

He, Men, Zhao, Lu and Ding [92]:

$$k_{nf} = k_{bf}\,(125.62\emptyset^2 + 4.82 + 1) \tag{73}$$

Table 4 below summarises the respective percentage error for each model for volume fractions lower than 1%, compared to the basic Maxwell model:

Table 4: Comparison of thermal conductivity models

Model	Percentage error compared to Maxwell
Maxwell-Garnett	0.458
He et al.	2.56
Buongiorno	1.646

From Table 4, it is evident that, for low volume fractions, the effect of the model on the estimation is not significant. The equation presented by He et al. [91] is based on experimental results on TiO_2 water-based nanofluids. Due to this fact, the model of He et al. [91] is chosen to obtain the thermal conductivity of the nanofluid investigated in this study.

Figure 4 below shows the thermal conductivity for different volume fractions over a temperature range of 278.15 K to 328.15 K.

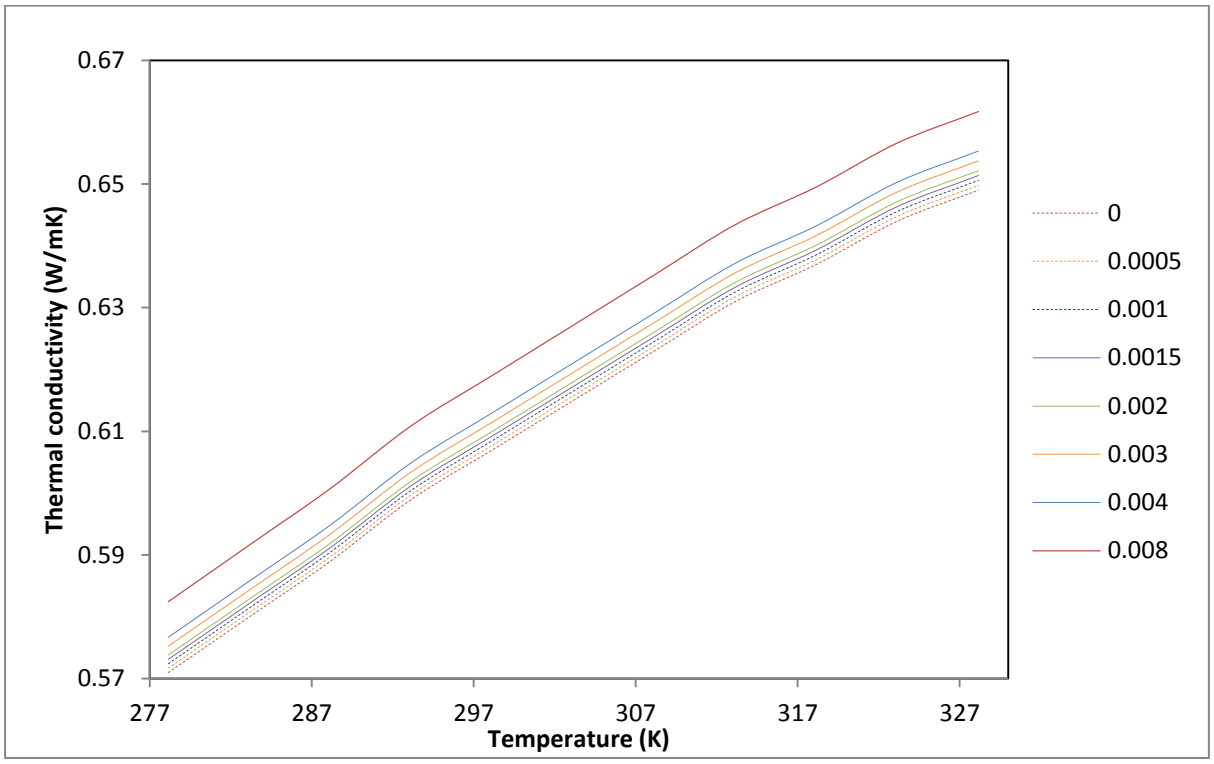

Figure 4: Thermal conductivity vs temperature for various volume fractions

As expected, the thermal conductivity increases as the temperature increases. It is also worth noting that thermal conductivity is also dependent on volume fraction, and increases with an increase in the volume of TiO_2 in the fluid (increase in volume fraction).

3.5.3 Density of the TiO_2 nanofluid

As with most nanofluid properties, the density of the fluid can be predicted by different models. A journal article published by Sharifpur et al. [66] states that the type of nanoparticle (TiO_2 in this investigation) does not significantly affect the density, while the particle size has a direct influence on the density. The study also found that the error between different density models is insignificant for volume fractions lower than 1%.

Due to these findings, the suggested model was selected to estimate the density of the nanofluid for various volume fractions over a range of temperatures (equations 67 and 68 were used)

$$\rho_{nf} = \frac{\varphi_{nf}\rho_p + (1 - \varphi_{nf})\rho_{bf}}{(1 - \varphi_{nf}) + \frac{\varphi_{nf}(r_p + t_v)^3}{{r_p}^3}} \tag{74}$$

where,

$$t_v = -0.0002833{r_p}^2 + 0.0475r_p - 0.1417 \tag{75}$$

Figure 5 below shows the subsequent density for various volume fractions over the temperature range.

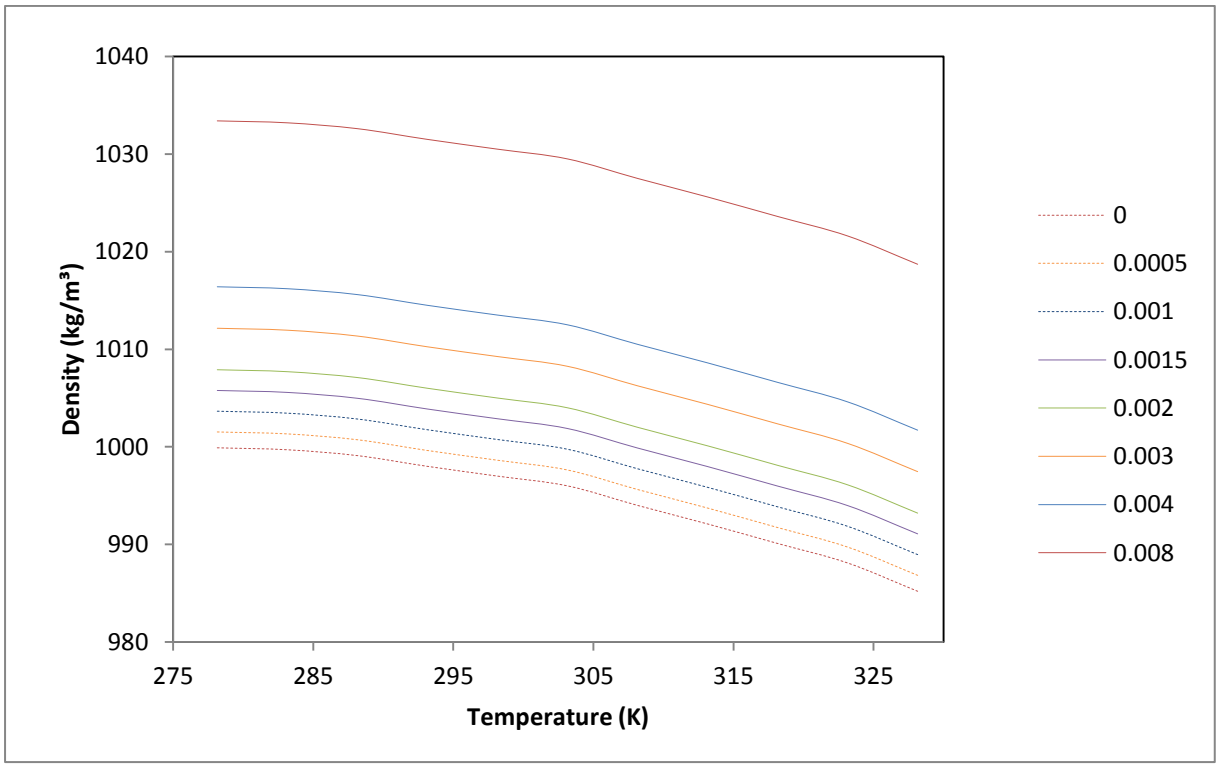

Figure 5: Density vs temperature for various volume fractions

From Figure 5 above, it is clear that density increases with an increase in volume fraction, but decreases as the temperature increases. The observed phenomenon is what was expected from the model equation.

3.5.4 Dynamic viscosity of the TiO_2 nanofluid

A fluid dynamic viscosity can be determined experimentally using a viscometer. To determine the dynamic viscosity of this specific nanofluid, the SV-10 vibro viscometer, shown in Figure 6, was used.

The device is described as a sine-wave vibro viscometer that achieves a high measurement accuracy (1% error) over its full range [93].

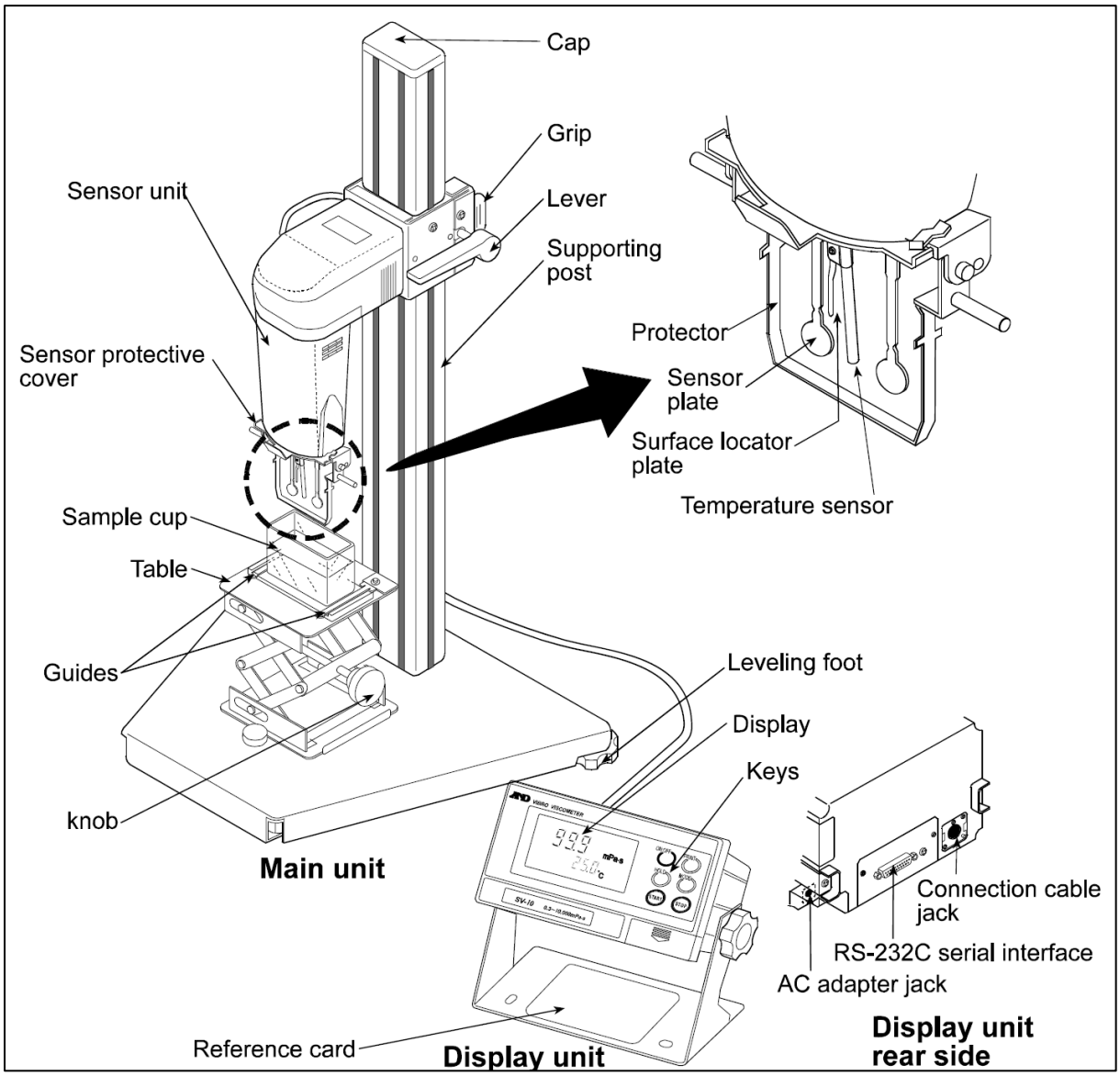

Figure 6: Schematic of the vibro viscometer SV-10 [93]

Before any measurements were taken for the nanofluid samples, the viscometer was calibrated using the method outlined in the user manual [93] using deionised water as the reference fluid. To determine the dynamic viscosity of a nanofluid, the sample preparation steps were followed as described in the SV-10 Vibro Viscometer Instruction Manual [93]. The temperature of the nanofluid was then ranged from 5 °C to 55 °C, while the respective viscosities were recorded. The temperature of the nanofluid could be altered by increasing or decreasing the temperature of the water circulated around the cup containing the nanofluid by using a thermal bath. The results are given in mPa.s and are logged on a computer. They can be exported in a Microsoft Excel format.

In Figure 7 below, the dynamic viscosity for the various volume fractions over the specific temperature range can be seen.

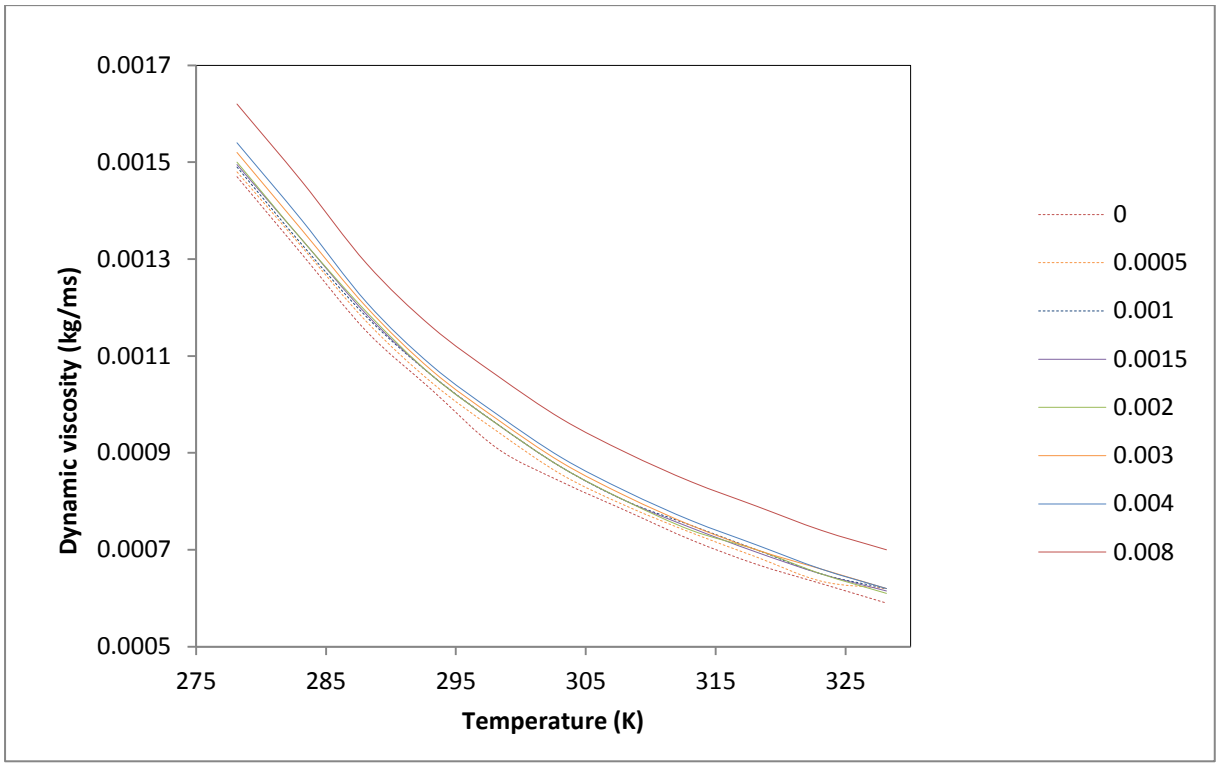

Figure 7: Dynamic viscosity vs temperature for various volume fractions

Figure 7 above shows that, as expected, the dynamic viscosity decreases as the temperature increases. The effect of the volume fraction on the dynamic viscosity (as predicted by the existing mathematical models) can also be observed.

When comparing the experimental results to the Brinkmann model designed to predict dynamic viscosity, an average percentage error of 0.2% is obtained. As this is a low error, it can be concluded that the experimentally determined dynamic viscosity results are accurate enough and can be used to define the nanofluid.

3.5.5 Specific heat capacity of the TiO_2 nanofluid

The specific heat capacity of the TiO_2 nanofluid is predicted using the model suggested by Ho et al. [64] using the equation:

$$\rho_{nf}\, C_{p,nf} = \varphi_{nf}\, \rho_p C_{p,p} + \left(1 - \varphi_{nf}\right)\rho_{bf} C_{p,bf} \tag{76}$$

Using the properties of the base fluid and the TiO_2 particles, the specific heat capacity is estimated for the volume fractions 0.05%, 0.1%, 0.15%, 0.2%, 0.3%, 0.4% and 0.8%.

The specific heat capacities are shown in Figure 8 below as opposed to the temperature of the nanofluid.

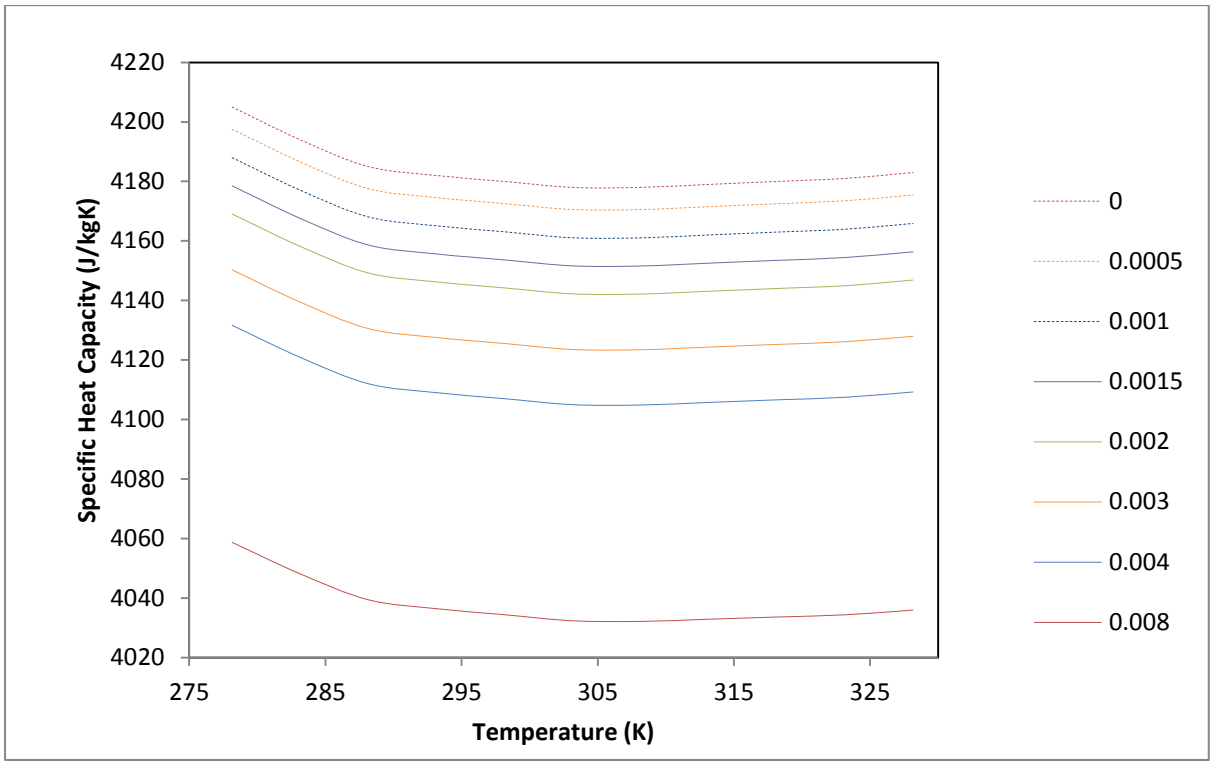

Figure 8: Specific heat capacity vs temperature for various volume fractions

3.5.6 Thermal expansion coefficient of the TiO_2 nanofluid

In the Heat and Mass Transfer textbook of Çengel and Ghajar [1], the volumetric expansion coefficient is defined as:

$$\beta = -\frac{1}{\rho}\left(\frac{\partial \rho}{\partial T}\right)_P \tag{77}$$

Ho et al. [65] give the two expressions for the coefficient of expansion (β) for a nanofluid. They report that the second equation provides a better correlation to experimental results.

$$\beta_{nf} = \varphi_{nf}\beta_p + (1 - \varphi_{nf})\beta_{bf} \tag{78}$$

$$\rho_{nf}\beta_{nf} = \varphi_{nf}\rho_p\beta_p + (1 - \varphi_{nf})\rho_{bf}\beta_{bf} \tag{79}$$

Figure 9 below is a graphic representation of the thermal expansion coefficient of the TiO_2 in deionised water for various volume fractions

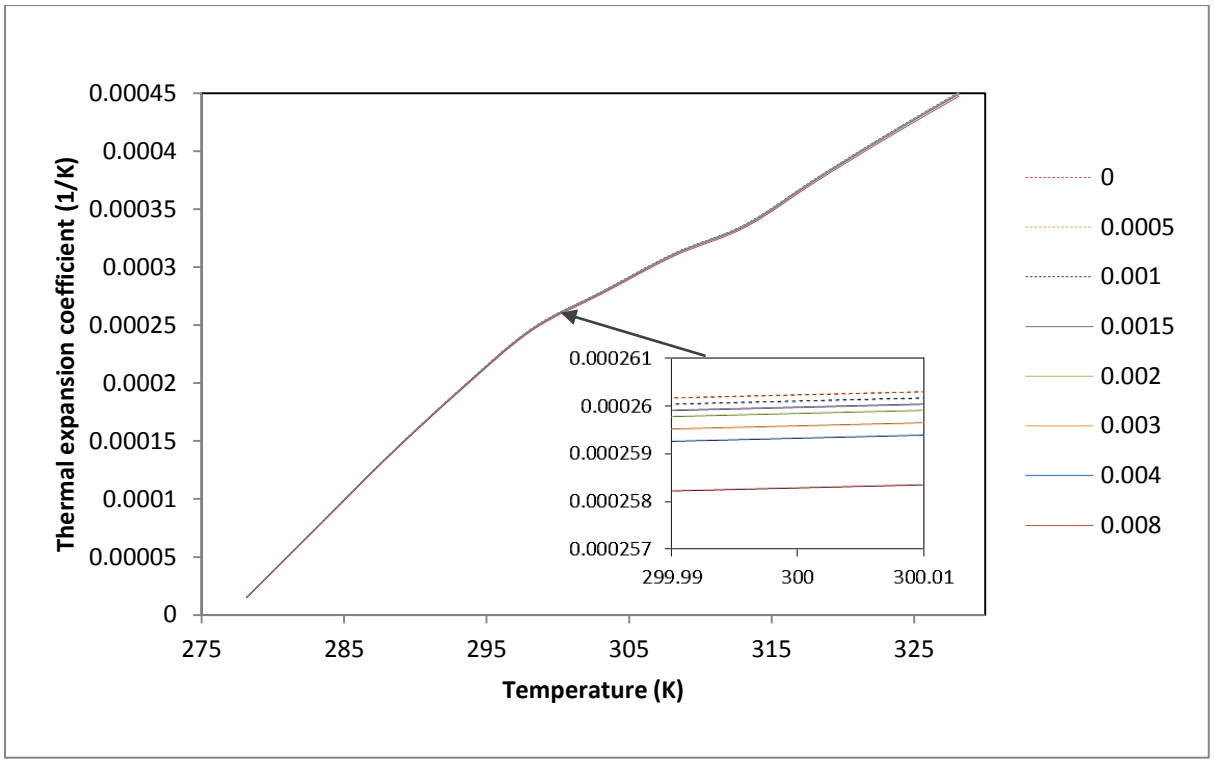

Figure 9: Thermal expansion coefficient vs temperature for various volume fractions

From the above figure, it can be concluded that the effect of the volume fraction on the thermal expansion coefficient is insignificant.

3.6 Experimental setup

The cavity used to investigate the heat transfer capabilities of the fluids has two heat exchangers. The thermal baths supplying these heat exchangers are switched on and the desired temperature is set. While the thermal baths are working to achieve this temperature, the cavity is thoroughly cleaned using deionised water so as not to contaminate it. When the cavity is clean, the nanofluid is poured into the cavity and the lid is placed on top to seal it from the surroundings.

Figure 10 below is a schematic drawing of the experimental setup:

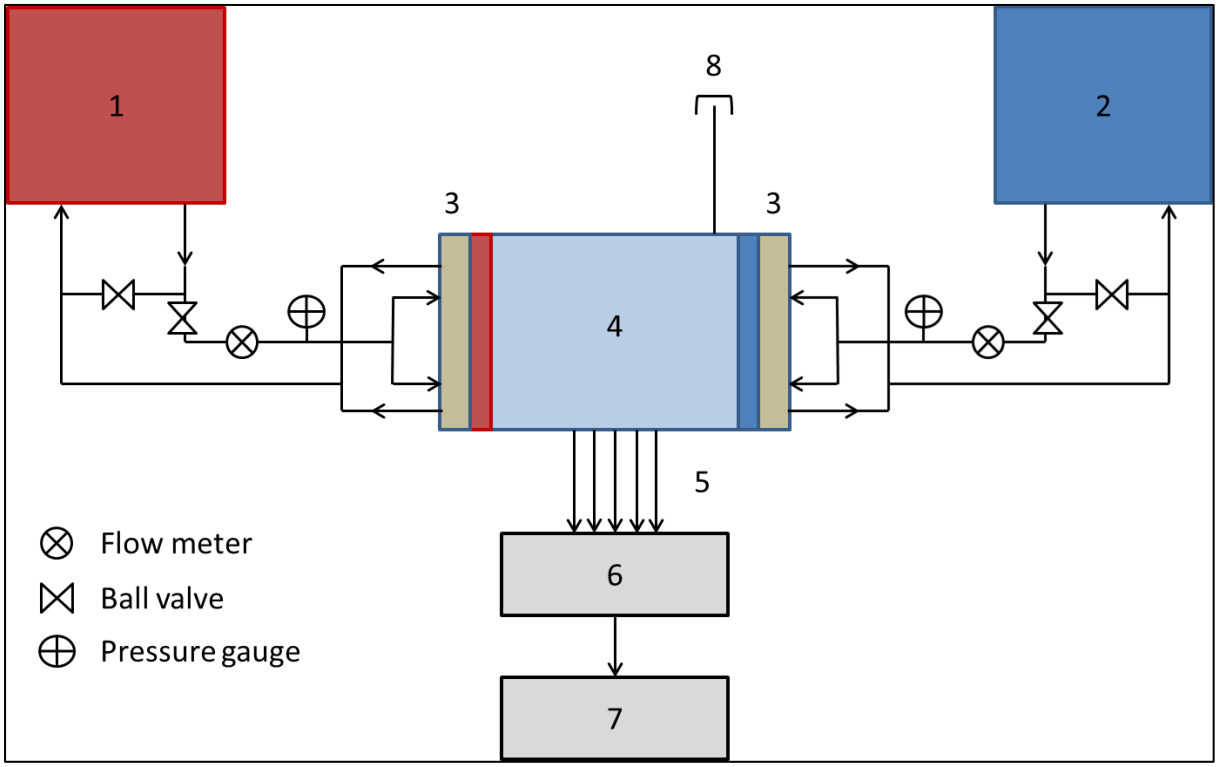

Figure 10: Schematic drawing of the experimental setup

In the figure above, the numbers point to the following items of the setup:

1. Thermal bath (hot)
2. Thermal bath (cold)
3. Copper heat exchanger
4. Test cavity (dimensions 96.3mm x 102.5mm x 120.04mm)
5. Thermocouples
6. Data logger
7. Computer
8. Cavity drainage system (including valve)

The experimental setup contains two thermal baths: one is set to a high temperature, while the other is set to a low temperature. Each thermal bath provides its own heat exchanger (represented by a black rectangle on both sides of the cavity) with two sources of temperature-controlled water. The thermal baths each receive the water leaving the heat exchanger, which is now at an altered temperature (higher for the low temperature and lower for the high temperature).

The heat exchangers are designed to accurately emulate walls of a constant temperature (the design is owned by the University of Pretoria). The other four walls of the cavity are manufactured from perspex/insulation. The entire cavity is surrounded by insulation with a thermal conductivity of 0.033 W/mK, as this minimises heat losses to the surroundings. Inside the cavity and at the inlets and outlets of the heat exchangers, T-type thermocouples (with an accuracy of 0.02 °C) are used to measure the temperature. The volume flow rate (fully developed flow was ensured through the placement of the flow meters) of water through the heat exchangers is measured using Burkert type

8081 ultrasound flowmeters. These flowmeters have an accuracy of approximately 2% and a repeatability of 1% over the range of 0.0666 to 0.3333 litres per second.

The information measured through the use of the thermocouples and flowmeters is logged using the National Instrument data logger SCXI-1303. The information is then recorded on a computer and can be saved in the form of Microsoft Excel data to simplify post-processing.

The placement of the thermocouples can be seen in Figure 11 below:

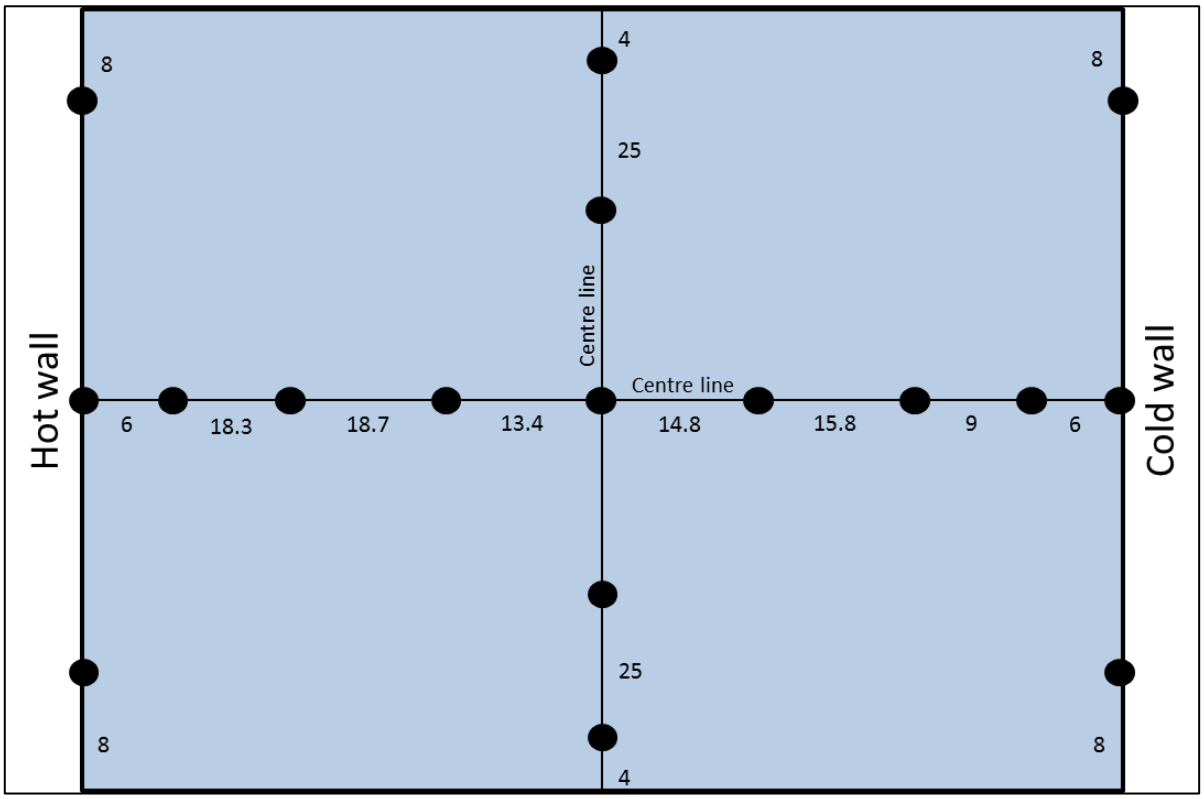

Figure 11: Schematic drawing showing the placement of the thermocouples within the cavity

In the figure above, each black dot represents a thermocouple and the dimensions are given in mm.

The figure below shows a photograph of the experimental setup,

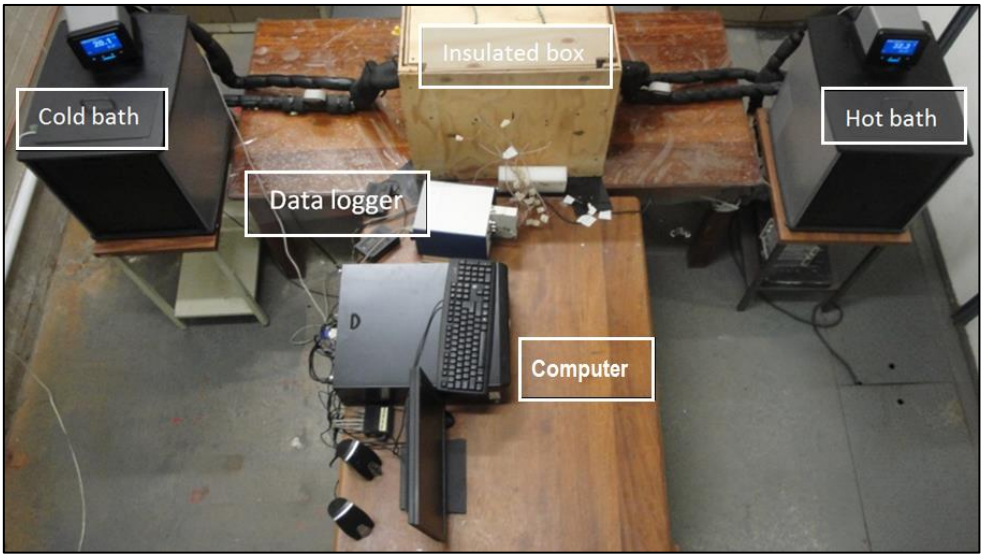

Figure 12: Experimental Setup (photograph)

In the photograph of the experimental setup, the hot and cold thermal baths can be seen as well as the insulted box containing the cavity used for the experiment. The Figure also shows the computer and the data logger to capture data.

3.7 Experimental procedure

When conducting the experiments, the procedure is followed as set out below:

- Preparation: the nanofluid sample was prepared according to the methodology depicted in Section 3.3
- Stability: stability is checked as described in Section 3.4
- Properties of the nanofluid: the properties of the specific volume fraction of the nanofluid are determined experimentally or using proven models as described in Section 3.5
- Heat transfer experiment

To determine the heat transfer capacity of the nanofluid, a heat transfer experiment is designed.

A cavity with one cold wall (heat exchanger connected to a thermal bath), one hot wall (heat exchanger connected to a thermal bath) and four insulated walls is used.

- The prepared, stable nanofluid, of which the thermal physical properties have been determined, is placed in the cavity.
- The inlet temperatures of the heat exchangers, representing the hot and the cold walls, are specified through the use of the thermal baths.
- The temperature of the water is measured at the inlet and outlet of both heat exchangers.
- The temperatures within the cavity, as well as those of the water flowing through the heat exchangers, are monitored to determine when steady state has been achieved.

- Once steady state has been reached (usually after 45 minutes), 1 000 sample points (of the temperature of the water at the inlet and outlet of both heat exchangers, as well as the flow rates through the heat exchangers) are recorded and saved.
- The heat transfer is not measured directly, but calculated using the following equation:

$$q = \dot{m} C_p \Delta T \tag{80}$$

  Where $\dot{m}$ is the mass flow rate (which is measured using a Burkert type 8081 ultrasound flowmeter), C_p is the specific heat capacity of water and ΔT is the temperature difference between the water entering the heat exchanger and the water exiting the heat exchanger (the temperatures are measured using T-type thermocouples within the inlet and outlet pipes of the heat exchanger).
  (The above procedure was used for each heat exchanger and the average between was used as the heat transfer rate for the system.)
- The heat lost by the system can be determined by calculating the difference between the heat transferred by the two separate heat exchangers (for a perfect system, the heat lost would be zero).

The heat transfer was determined for different temperature combinations. These combinations are shown in Table 5 below:

Table 5: Temperature combinations for experiments

Temperature cold (°C)	Temperature hot (°C)	Temperature difference (°C)
5	55	50
10	50	40
15	45	30
20	40	20

3.7.1 Volume fractions

The nanofluid was prepared for different volume fractions. The following volume fractions were prepared and investigated experimentally:

- 0% (deionised water – base fluid without nanoparticles)
- 0.05%
- 0.1%
- 0.15%
- 0.2%
- 0.3%
- 0.4%
- 0.8%

The results could then be analysed to determine the optimum volume fraction at which the peak heat transfer occurred.

The same method as described above is used for all the volume fractions.

3.8 Data reduction

From the experiments, the data recorded was analysed and calculations were performed to obtain the heat transfer, heat transfer coefficient, Rayleigh number and Nusselt number. The information is presented below in the form of graphs to facilitate a comparison between the different volume fractions and temperature differences.

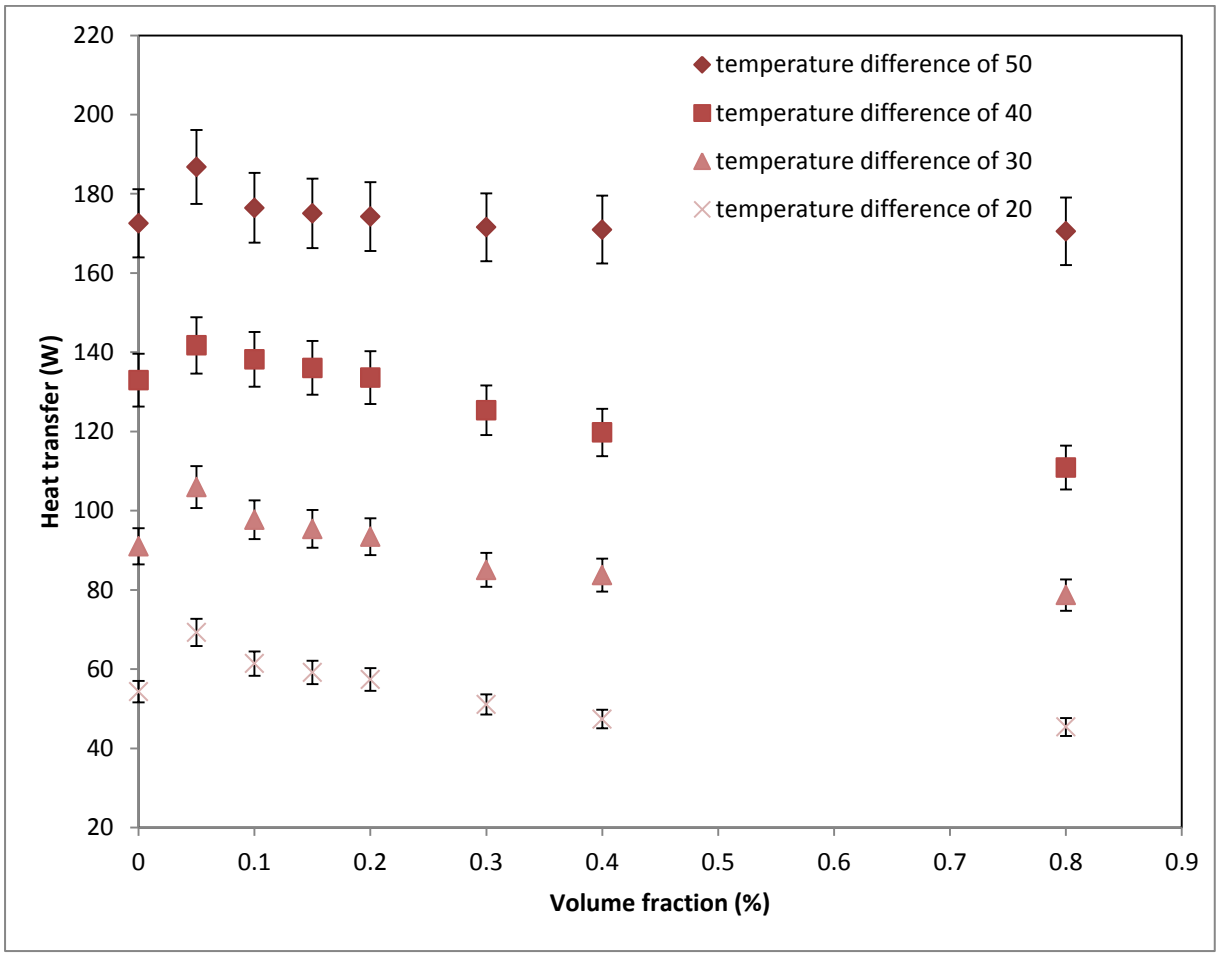

Figure 13: Heat transfer vs volume fraction for various temperature differences (experimental)

From Figure 13 above, it is clear that, as the temperature difference increases, the heat transfer increases. This phenomenon follows an expected trend, as the heat transfer is directly dependent on the temperature difference.

Analysing the data, it is also observed that the heat transfer varies with the volume fraction. The heat transfer increases with an increase in the volume fraction and achieves peak heat transfer at 0.05%. After this, as the volume fraction is increased, the heat transfer reduces to a level lower than that of pure deionised water.

The maximum heat transfer takes place at a volume fraction of 0.05% and a temperature difference of 50 °C. This is thus the optimum volume fraction.

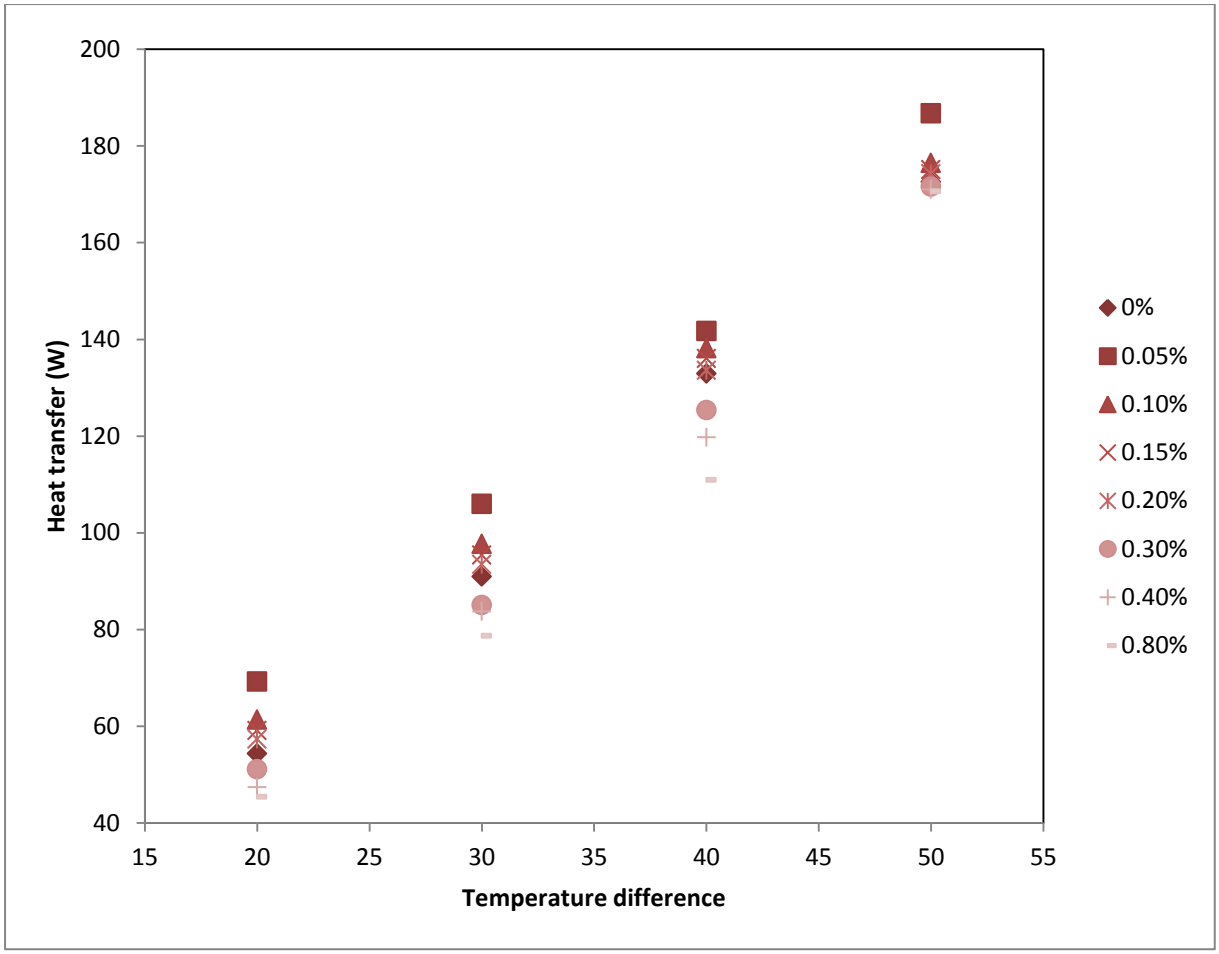

Figure 14: Heat transfer vs temperature difference for various volume fractions (experimental)

Figure 14 above visually depicts the heat transfer vs volume fraction for the different temperature differences. As expected, the heat transfer is directly proportional to the temperature difference between the two temperature-controlled walls. The heat transfer increases (with an almost linear relation) as the temperature difference between the walls increases. The highest heat transfer is obtained with the TiO_2 nanofluid with a volume fraction of 0.05%. The same observation was made when analysing the graph showing the heat transfer as a function of the volume fraction.

Using the equations detailed in Section 2.2, the Nusselt number and the Rayleigh number are calculated and shown in Figure 15 below.

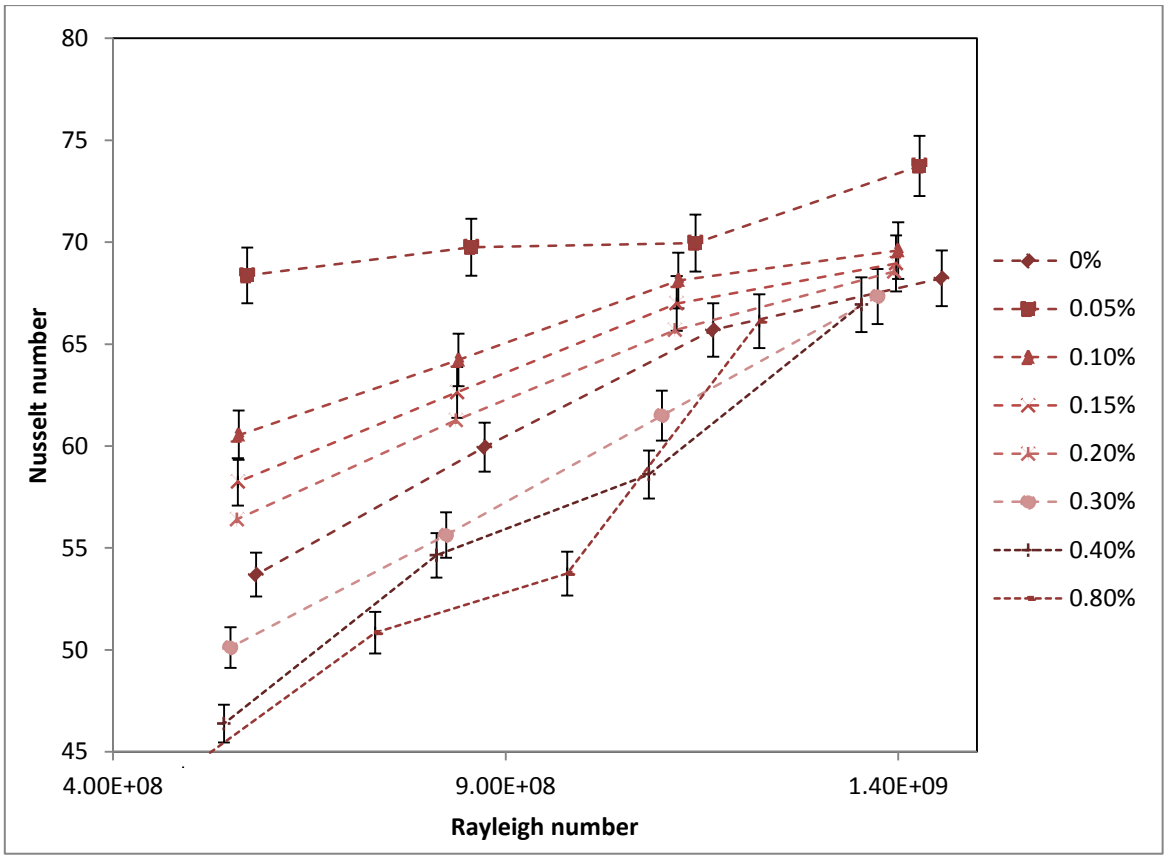

Figure 15: Nusselt number vs Rayleigh number for various volume fractions

From Figure 14 above, it is clear that the Nusselt number increases as the Rayleigh number increases for each volume fraction. The experiments were done over a Rayleigh number range of 4.89e + 8 to 1.46e + 10.

3.8.1 Uncertainty analysis

When analysing results obtained through experimental studies, it is important to know the uncertainty, or error, that accompanies these results. An uncertainty analysis was completed to determine the reliability of the results.

The experimental measurements that affect the results the most are the measurement of the temperature and the flow rate.

To determine the uncertainty level, the following equations are used:

$$\delta Q = \left(\left(\frac{\delta Q}{\delta \dot{m}} \delta \dot{m} \right)^2 + \left(\frac{\delta Q}{\delta c_{p_{bf}}} \delta c_{p_{bf}} \right)^2 + \left(\frac{\delta Q}{\delta T_h} \delta T_h \right)^2 + \left(\frac{\delta Q}{\delta T_c} \delta T_c \right)^2 \right)^{\frac{1}{2}} \quad (81)$$

$$\delta h = \left(\left(\frac{\delta h}{\delta Q} \delta Q \right)^2 + \left(\frac{\delta h}{\delta A} \delta A \right)^2 + \left(\frac{\delta h}{\delta T_h} \delta T_h \right)^2 + \left(\frac{\delta h}{\delta T_c} \delta T_c \right)^2 \right)^{\frac{1}{2}} \quad (82)$$

$$\delta Nu = \left(\left(\frac{\delta Nu}{\delta h} \delta h \right)^2 + \left(\frac{\delta Nu}{\delta L_c} \delta L_c \right)^2 + \left(\frac{\delta Nu}{\delta k_{eff}} \delta k_{eff} \right)^2 \right)^{\frac{1}{2}} \quad (83)$$

Using the above equations, the maximum uncertainty was determined: 5.3% for the heat transfer, 5.3% for the heat transfer coefficient and 4.62% for the Nusselt number.

The calculated uncertainty is included in the results in the form of error bars.

3.9 Conclusion and recommendations of the experimental investigation

This section contains the author's conclusion on the experimental investigation, as well as all recommendations made by the author.

3.9.1 Conclusion of the experimental investigation

This section focusses on the experimental investigation of the heat transfer capabilities of a TiO_2 nanofluid.

The safety aspects involved in conducting experiments with nanofluids are discussed and recommendations on the suggested safety precautions are explained. The methodology followed to prepare a stable form of the TiO_2 water-based nanofluid is explained. The properties of the nanofluid are either tested experimentally using special equipment or determined using known mathematical or empirical models.

Using a carefully designed experimental setup and experimental procedure, the decided parameters are tested. The results are discussed and an uncertainty analysis is conducted to determine the accuracy and reliability of the experimental investigation.

Results showed that the heat transfer increased with an increase in temperature and that an increase (8.2%) in the heat transfer compared to that of the base fluid is obtained at the optimum volume fraction. It was concluded that the nanofluid allowed for the maximum heat transfer of 186.76 W at a volume fraction of 0.05% and a temperature difference of 50 °C.

3.9.2 Recommendations made from the experimental investigation

It is the author's recommendation that the experimental investigation is furthered by including a study into the dependency of the heat transfer on the nanoparticle size (radius). Another aspect of the investigation that can be expanded is that of the influence of different material nanoparticles instead of the TiO_2 particles.

The dependency of heat transfer on particle size and particle material could be an invaluable contribution to this investigation. The effect of the cavity dimensions on the heat transfer should also be investigated.

4. Numerical investigation

4.1 Introduction to the numerical investigation

The numerical Investigation is performed to confirm the results of the experimental investigation. Identical cases as were investigated experimentally are modelled numerically using the commercially available CFD software, ANSYS-FLUENT version 17.0.

4.2 Defining the problem for the numerical investigation

The TiO_2-deionised water nanofluid is investigated numerically. The numerical investigation is done in the form of several simulations of the nanofluid in specific situations.

When modelling a nanofluid, two different methods are generally used. The first method is the multi-phase model, where the nanofluid is depicted as a base fluid with small particles suspended in it. This method is complex and computationally expensive as each particle is modelled separately.

The second method, single-phase modelling, consists of modelling the nanofluid as a fluid with altered properties. Using this method, the nanofluid is imagined as a new material in the liquid phase with specified properties. The single-phase method is a simple way of modelling the fluid with sufficient accuracy without allowing the simulation to become computationally too expensive.

For this investigation, the single-phase method is used to model the nanofluid to allow for a comparison to previously obtained experimental results.

4.3 Geometry of the numerical investigation

The first step of the CFD analysis was to create the geometry that represents the system at hand. This section explains the details behind the geometry that is used for this study.

4.3.1 A two-dimensional model to investigate the three-dimensional case

The geometry pertaining to the investigation is that of a rectangular cavity (3D). According to a study performed by Mahdavi, Ghodsinezhad, Sharifpur and Meyer [94], a two-dimensional (2D) cross-section of the cavity can be used as an accurate representation of the cavity.

The study involved modelling the cavity at hand filled with air as a full 3D system with heat exchangers, as a 3D cavity with constant wall temperatures and as a 2D cross-section with constant wall temperatures. The results were then compared to experimental results.

The study concluded that the error involved in modelling the system as a simple cavity was less than 5%. The same observation was made when the system was modelled as a 2D cross-section.

Due to the discoveries made by Mahdavi et al [94], the system in the current investigation can be modelled as a 2D geometry.

4.3.2 Basic geometry generation

The 3D experimental cavity is modelled in two dimensions. A cross-section of the cavity is used to represent the entire cavity. A representation of the geometry with the dimensions 102.5 mm x 96.3 mm can be seen in Figure 16 below,

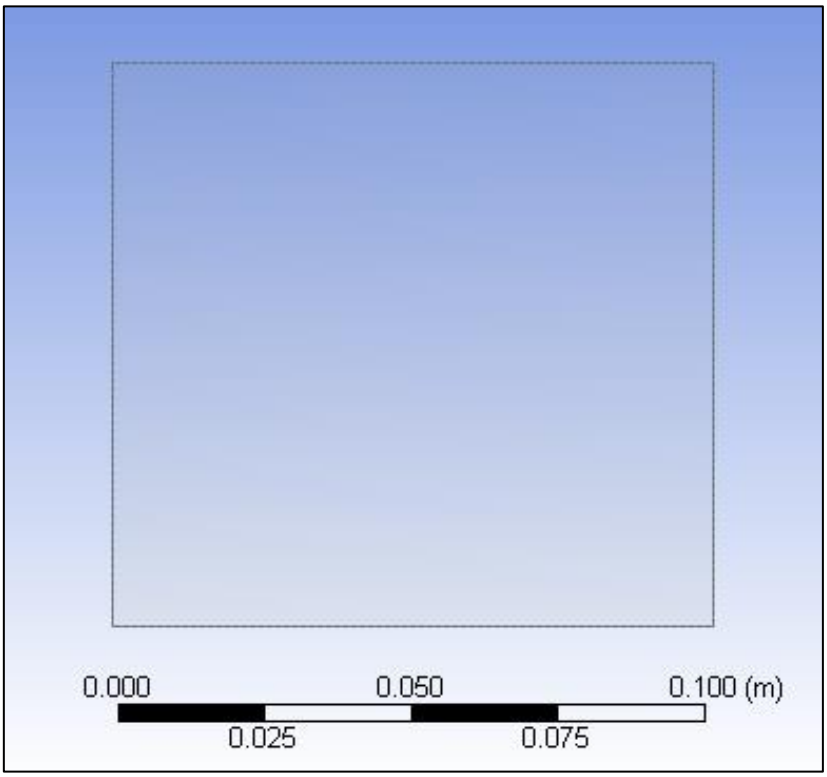

Figure 16: Two-dimensional geometry representing the cavity

The above figure shows the basic geometry, which represents a 2D cross-section of the experimental cavity.

4.4 Boundary and initial conditions

To accurately define the case that it to be investigated, the conditions at the boundaries of the investigation (in this case the walls) and at the start of the investigation (initial conditions) need to be explained and defined. These conditions are explained and defined in this section.

4.4.1 Boundary conditions of the numerical investigation

The student considered investigating the effect that different boundary conditions would have on the final solution. Due to the fact that specific boundary conditions are recommended by ANSYS-FLUENT for the modelling of natural convection in a cavity, this analysis was considered redundant and not performed.

The following boundary conditions were assigned to the geometry:

- Cold wall – wall: stationary, no slip, constant temperature
- Hot wall – wall: stationary, no slip, constant temperature
- Top wall – wall: stationary, no slip, constant heat flux (zero)
- Bottom wall – wall: stationary, no slip, constant heat flux (zero)
- Fluid – interior-fluid: nanofluid

The above boundary conditions are as suggested in the ANSYS-FLUENT tutorial, *Modelling Radiation and Natural Convection,* available as part of the commercial software package.

4.4.2 Initial conditions of the numerical investigation

The initial conditions of an investigation define the state of the system at hand at the start of the analysis. As four different cases were modelled in this case, the initial conditions of these cases are summarised in Table 6 below,

Table 6: Initial conditions for the four cases

Case (temperature difference)	Cold wall temperature (K)	Hot wall temperature (K)
1 (50K)	278.15	328.15
2 (40K)	283.15	323.15
3 (30K)	288.15	318.15
4 (20K)	293.15	313.15

In each case, the hot and cold walls were depicted as walls with no slip conditions and a specified constant wall temperature.

4.5 Modelling the material properties of the nanofluid

As the single-phase method is used to model the nanofluid for this investigation, a new fluid was defined in ANSYS-FLUENT. As the nanofluid's properties are dependent on the volume fraction, each volume fraction simulated for this investigation was treated as a separate fluid, and thus a fluid was created for each. The nanofluid is defined by the properties density, specific heat capacity, thermal conductivity, dynamic viscosity and thermal expansion coefficient.

For each volume fraction the properties of the nanofluid were determined as in the experimental investigation, and explained in Section 3.5. Within the CFD software, the density was modelled using the Boussinesq equation. A Boussinesq approximation was chosen to model the density as it is valid for natural convection cases with little temperature change, and the fluid flow is buoyancy driven. The model treats density as a constant in all terms in the momentum equation except for the buoyancy term, and can be explained by the equation:

$$(\rho - \rho_0)g \approx -\rho_0\beta(T - T_0)g \tag{84}$$

where the initial density (ρ_0) is at the cold wall temperature of T_0.

The other properties were defined using equations. Table 7 below summarises how the properties were modelled:

Table 7: Modelling the material properties

Property	Modelling method	Input
Density	Boussinesq	Density at the cold wall temperature
Specific heat capacity	Polynomial equation	Coefficients of the polynomial
Thermal conductivity	Polynomial equation	Coefficients of the polynomial
Dynamic viscosity	Polynomial equation	Coefficients of the polynomial
Thermal expansion coefficient	Constant	Property at the average temperature (30 °C)

The methods explained in the table above were used for each volume fraction. In the cases where a polynomial equation was used to model the property, a sixth-order polynomial that is dependent on temperature was used with a minimum R^2- value fit of 0.998 to the original property model. It was decided to use a constant to model the thermal expansion coefficient as the property does not vary much with temperature.

4.6 Models and solvers used in the numerical investigation

When performing simulations using CFD software, the user has to select the models that should be applied in solving the problem. Using the CFD software ANSYS-FLUENT, the following categories of models are available for use:

- Multiphase
- Energy
- Viscous
- Radiation
- Heat exchanger
- Species
- Discrete phase
- Solidification and melting
- Acoustic

As it was decided to use the homogenous model (single-phase model), the multiphase model will not be activated for this investigation. The heat exchanger, radiation, species, discrete phase, solidification and melting, and acoustic models will not be used for these simulations either.

For the viscous model, the realisable k-epsilon model with enhanced wall treatment was selected. Many different turbulence models were tested (laminar, k-epsilon standard, k-epsilon realisable, k-omega standard, k-omega SST), but it was found that the k-epsilon standard model with enhanced wall treatment obtained the most accurate measurement.

As with the model, different solvers were also tested. With this investigation, the aim was to find a solver for which the solution converged. In all cases, it was specified that the pressure equation should be driven by body forces. It was discovered that, for 2D simulations, as in this case, the coupled (pseudo-transient) solver should be used, as it is the most effective.

4.7 Mesh generation and validation for the numerical investigation

For all CFD investigations, the specified geometry is divided into cells. The software then analyses the geometry, one cell at a time, to obtain the final solution. The collection of cells that form the geometry is referred to as the mesh.

A general observation states that the more cells are used, the more accurate the solution. However, due the amount of calculations that go hand in hand with achieving this accuracy, the computational cost increases with accuracy. The computational cost of a simulation depends on the memory required for the calculations to be performed, as well as the time required to obtain a converged solution.

An optimum number of cells is to be found that allows for sufficient accuracy while minimising the computational cost.

4.7.1 Mesh generation

The mesh was generated using the meshing tool available in ANSYS-FLUENT. Edge sizing was used, specifying the number of cells or the element size.

Along the width of the geometry, a minimum element size of 0.0005 m was specified. A bias (short on the edges and long in the centre) and a bias factor of 5 were enforced. This was done to focus the computational power of the simulation towards the edges where the heat is introduced into the system (i.e. the hot wall and the cold wall). The bias factor was defined using a parameter, which could easily be changed without having to regenerate the mesh.

For the height, the number of cells was specified (varied for the mesh independence study). This was also done using a parameter to simplify the mesh independence study and grid convergence index investigation that follows in the next section.

Lastly, face meshing was used. After specifying the edge sizing, face mesh was selected to mesh the geometry using a quadrilateral mesh.

Figure 17 below shows an example of a mesh.

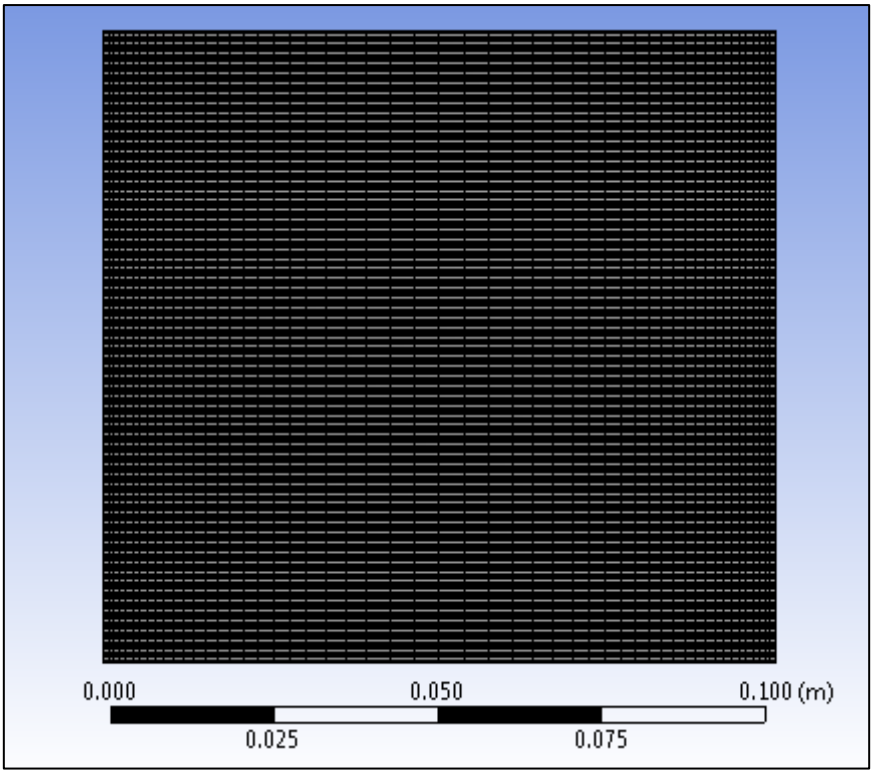

Figure 17: The meshed geometry

In the figure above, the inflation on the hot and cold walls (right and left) can clearly be seen, as well as the uniform cells along these walls.

4.7.2 Mesh quality

Once a mesh has been created, it is important that the quality of the mesh is inspected. The ANSYS-FLUENT function Mesh Quality was used to obtain the minimum orthogonal quality and the maximum orthogonal skewness.

The orthogonal quality can range from 0 to 1, where 1 represents a good quality mesh. The orthogonal skewness also ranges from 0 to 1. However, a good-quality mesh will have a maximum orthogonal skewness closer to 0.

For all the meshes generated for this investigation, the mesh quality was checked. It was found that, for all cases, the minimum orthogonal quality was 1 and the maximum orthogonal skewness was 0. Due to these findings, it was concluded that the quality of each of the meshes was good.

4.7.3 Mesh dependence study

Before the results obtained from the simulations can be accepted and further analysed, it is important to perform a mesh independence study. This study is done to ascertain if a solution is independent of the mesh used to obtain it or not.

For this investigation, the number of cells along the height was varied, as well as the minimum cell size along the width.

The results from the mesh independence study are summarised in Table 8 below:

Table 8: Results from the mesh independence study

	Number of cells – height	Minimum cell size (mm) – width	Number of cells	Heat transfer (W)	Percentage difference
Case 1	500	0.005	10 500	182.201	0.016
Case 2	250	0.005	5 250	182.23	0
Case 3	500	0.002	26 000	182.196	0.019
Case 4	250	0.002	13 000	182.276	0.025

From the results shown in the table above, it is observed that the heat transfer coefficient is very similar for all four cases, as shown by the small percentage difference. It can thus be concluded that the solution is independent of the mesh.

4.7.4 Grid convergence index

A method of checking the mesh independency is to calculate the Grid Convergence Index (GCI) for the mesh. The grid refinement ratio (r) for this case was 2. Using this ratio and the data obtained from three different simulations, the GCI ratio was calculated using the following equations:

$$p = \frac{\ln\left(\frac{f_3 - f_2}{f_2 - f_1}\right)}{\ln(r)} = 2.211 \tag{85}$$

$$GCI_{12} = \frac{F_s \left|\frac{f_2 - f_1}{f_1}\right|}{r^p - 1} = 0.001343 \quad GCI_{23} = \frac{F_s \left|\frac{f_3 - f_2}{f_2}\right|}{r^p - 1} = 0.006197 \tag{86}$$

$$\frac{GCI_{23}}{r^p\, GCI_{12}} = 0.996 \approx 1 \tag{87}$$

In the above calculations, f was taken to be the heat transferred.

Because the GCI was calculated to be approximately 1, it can be said that the solution is independent of the mesh.

The results of the mesh independence study and the GCI show that the coarsest mesh among the three shows enough accuracy, while being computationally cheaper. This mesh will be used for all further simulations.

4.8 Validating the results obtained through the numerical investigation

In the previous sections, it was proven that the results of the simulations were not dependent on the mesh used to obtain them. These results are to be validated by comparing them to the experimental results.

The validation is firstly done for the base fluid only (0%). Figure 18 below shows the experimental and numerical results of deionised water for various temperature differences.

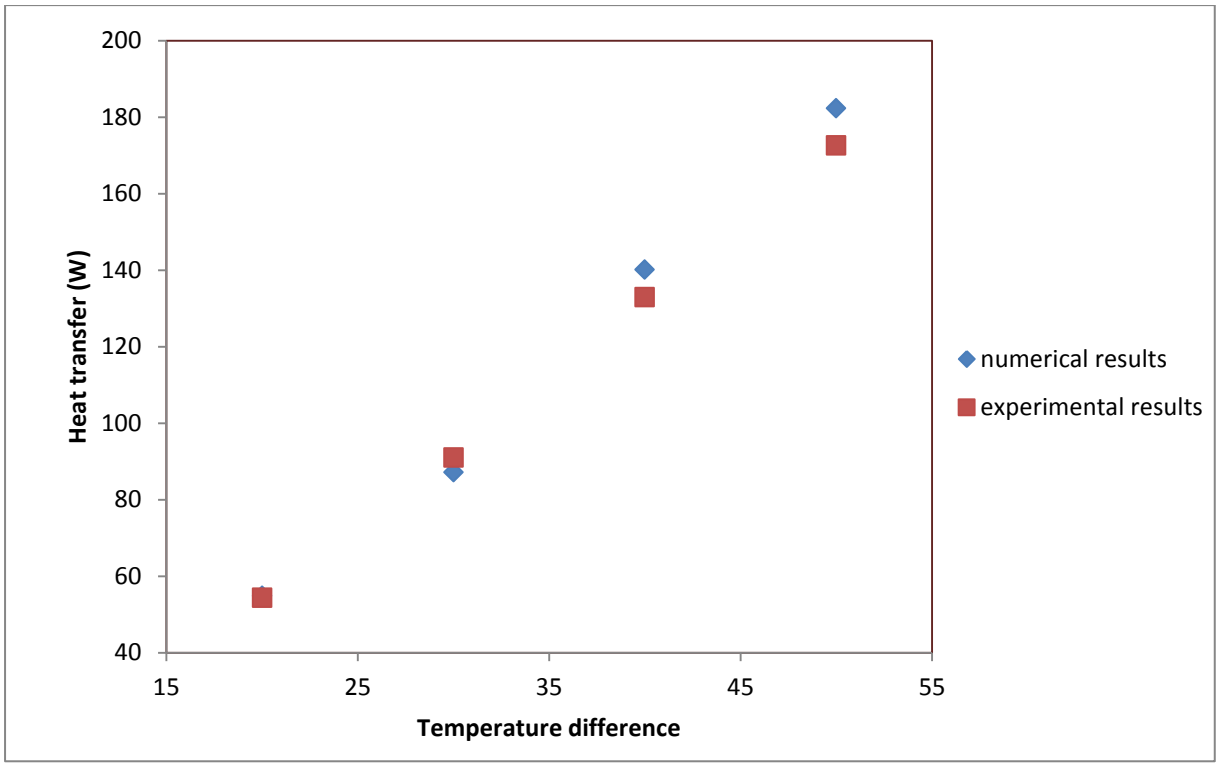

Figure 18: Heat transfer vs temperature difference for the base fluid (numerical and experimental results)

The numerical and experimental results show good correlation with the percentage difference, increasing slightly as the temperature difference increases. This increase in the error, to a maximum error of 5.6%, can be attributed to the heat lost from the experimental system, which is not modelled in the numerical system, as it is assumed to be perfect.

Once the model is validated for the base fluid, a validation is done for the nanofluid. Figure 19 below once again shows the heat transfer for various temperature differences, but in this case it shows the heat transfer for a volume fraction of 0.2%

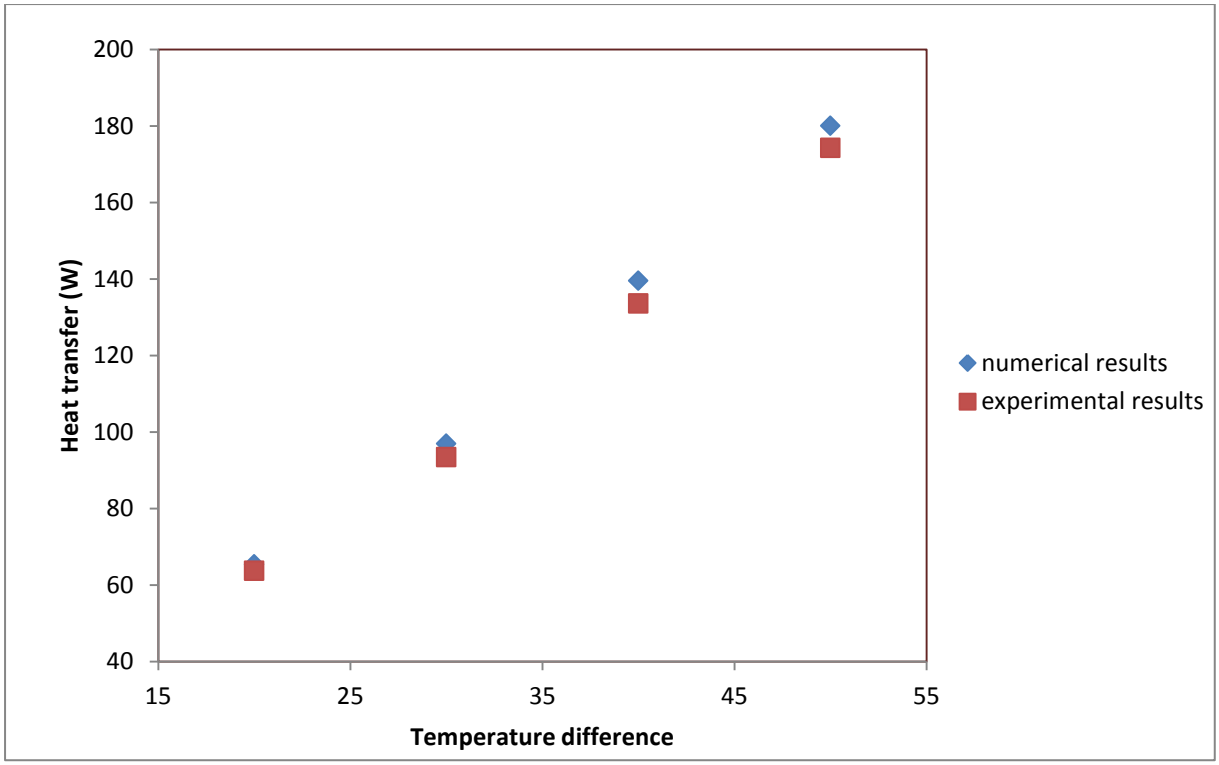

Figure 19: Heat transfer vs temperature difference for a volume fraction of 0.2% (numerical and experimental results)

The results once again show a good correlation between the numerical and experimental results. For this case, the error difference also increases (to a maximum difference of 4.3%) as the temperature difference increases. This error can again be explained by the heat loss that occurs from the experimental system, but is not included in the numerical modelling of the system.

Due to the correlation shown for both the base fluid and the 0.2% volume fraction nanofluid, the numerical model can be assumed to be sufficiently accurate in modelling the experimental system.

4.9 Simulations performed as part of the numerical investigation

In the preceding sections, the numerical model, as well as the results obtained from it, were validated and proven to be sufficiently accurate in modelling the experimental system. More simulations were performed with the following conditions:

Temperature difference of:

- 50K: 328.15K (hot wall) and 278.15 (cold wall)
- 40K: 323.15K (hot wall) and 283.15 (cold wall)
- 30K: 318.15K (hot wall) and 288.15 (cold wall)
- 20K: 313.15K (hot wall) and 293.15 (cold wall)

These temperature differences where tested for the volume fractions 0%, 0.05%, 0.1%, 0.15%, 0.2%, 0.3%, 0.4% and 0.8%

The testing conditions are the same as in the experimental investigation.

Once the numerical model had been set up, the solution was initialised using the hybrid initialisation method. The calculation was then started and the residuals (continuity, x-velocity, y-velocity, energy, k and epsilon) were plotted. Figure 20 below shows such a residual plot:

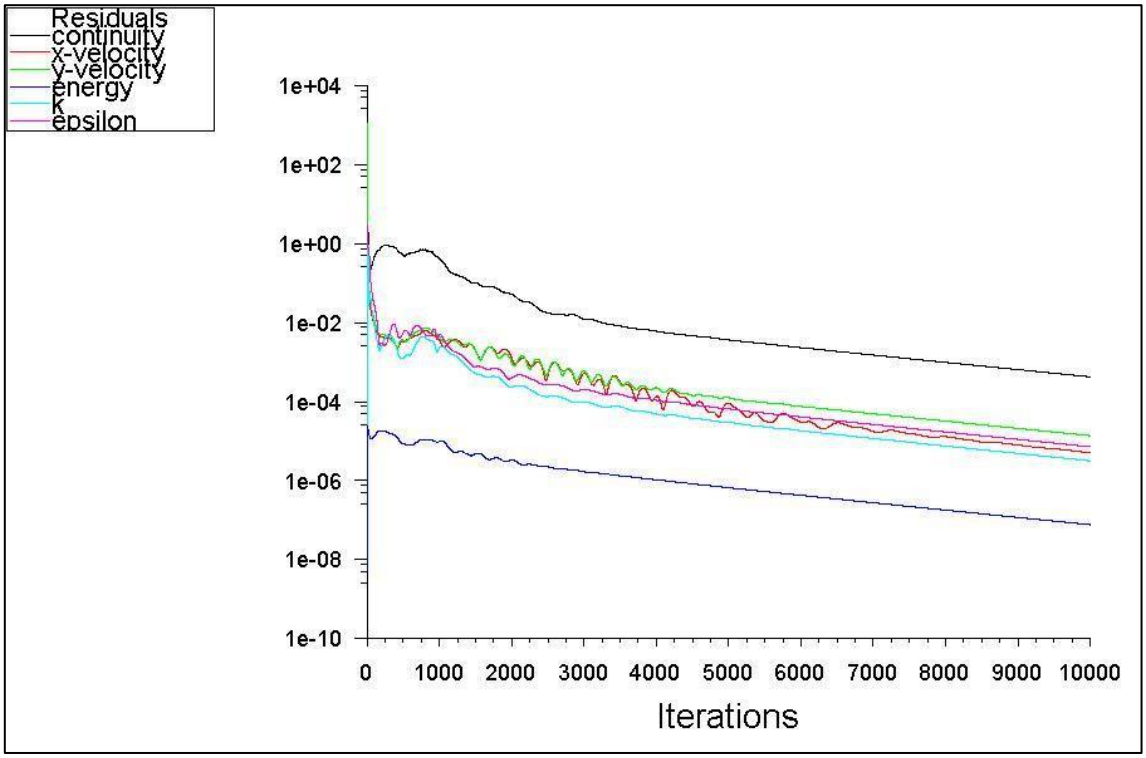

Figure 20: Residual plot for a numerical simulation

Once all the residuals had converged sufficiently (residuals below 0.001), the calculation was stopped.

The above methodology was followed for all simulations.

4.10 Results obtained through the numerical investigation

The simulations described in the previous sections were run and the results saved. Using the post-processing software included in the ANSY-FLUENT software, the results were analysed and presented in an easily understandable fashion.

Figure 21 below shows the heat transfer results obtained from the numerical investigations.

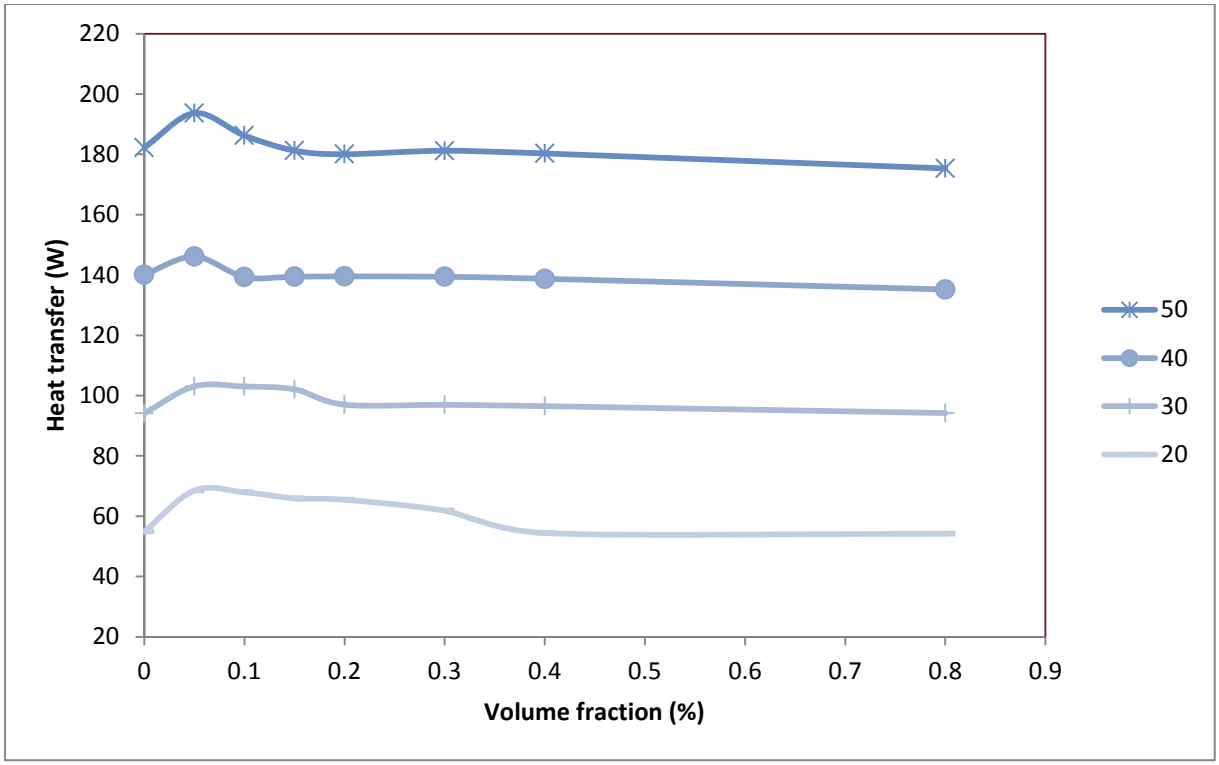

Figure 21: Heat transfer vs volume fraction for various temperature differences (numerical)

From the above figure, it can be seen that heat transfer increases as the volume fraction increases from 0 to 0.05%. As the volume fraction is increased further, the heat transfer reduces again. The heat transfer for volume fractions higher than 0.4% are, in some cases, even lower than the heat transfer achieved through pure deionised water. It is evident that the optimum volume fraction is 0.05% where the maximum heat transfer occurs.

Figure 22 shows the heat transfer vs temperature difference for different volume fractions.

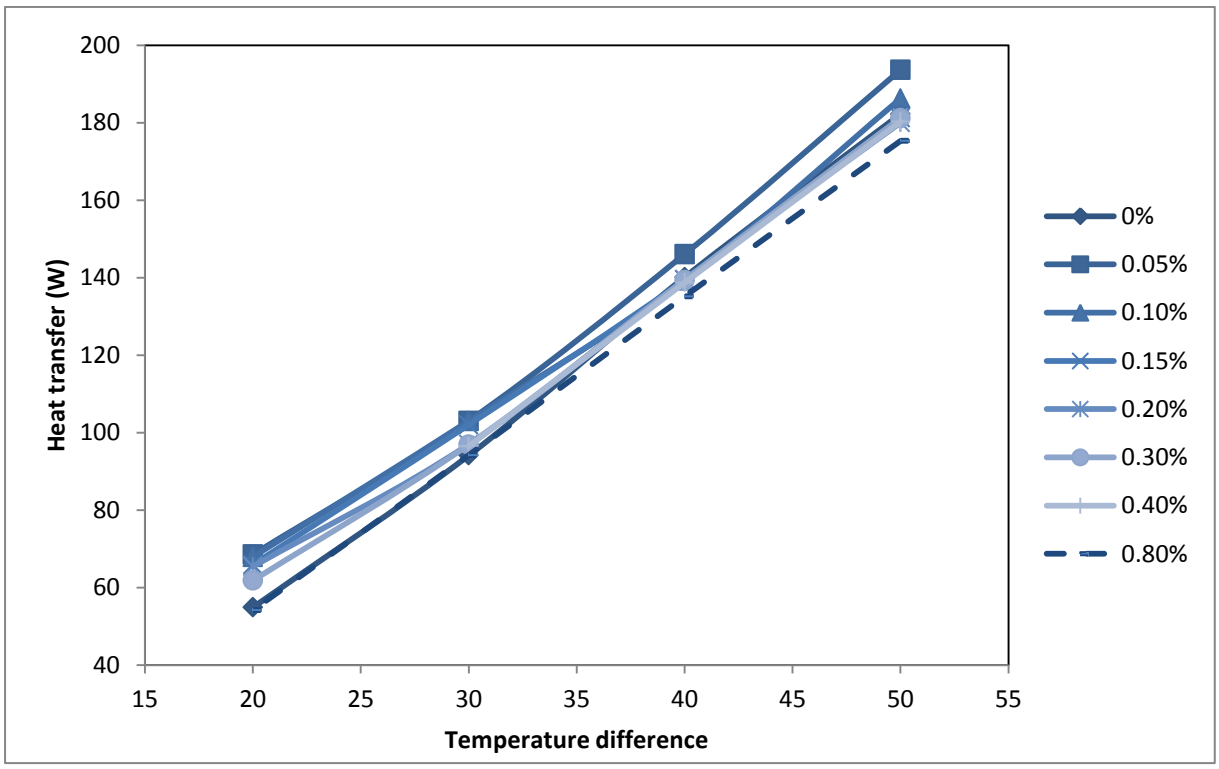

Figure 22: Heat transfer vs temperature difference for various volume fractions (numerical)

The figure above makes it clear that, as expected, heat transfer increases as the volume temperature difference is increased. It is also evident that the line depicting the volume fraction 0.05% is the highest for each temperature difference, once again proving that this is the optimum volume fraction for enhanced heat transfer.

Using the post-processing tool in ANSYS-FLUENT, contour plots at the optimum volume fraction could be depicted.

The temperatures seen on the static temperature contour plot range from 278.15 K (dark blue) to 328.15 K (red), with the minimum temperature occurring on the cold wall and the maximum temperature occurring on the hot wall. As the fluid increases in temperature, the density inadvertently decreases. The different fluid temperatures in the cavity cause buoyancy-driven flow as the lower density fluid rises to the top and the higher density fluid moves downward. This buoyancy-driven flow is a phenomenon of natural convection.

The buoyancy-driven flow explained previously can clearly be seen in the velocity contour plot. From the plot, it is evident that the majority of the fluid motion takes place close to the heated and cooled walls, where the fluid velocity reaches maximums of 0.00878 m/s. No fluid motion takes place in the centre of the cavity, while very low velocities can be noticed near the top and bottom barriers.

The static temperature and velocity contour plots of the 0.05% case are shown in Figure 23 and Figure 24.

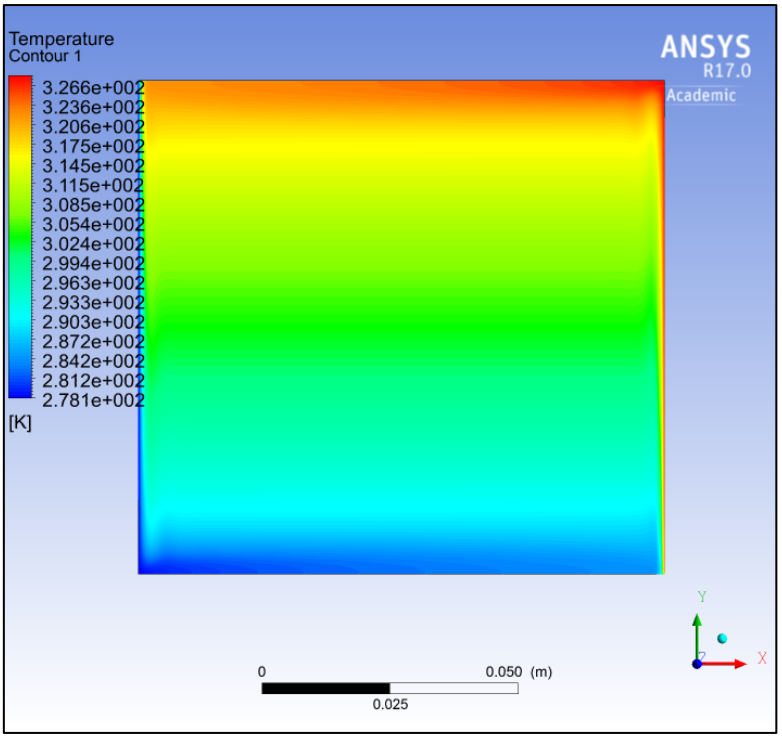

Figure 23: Static temperature contour plot for volume fraction 0.05%

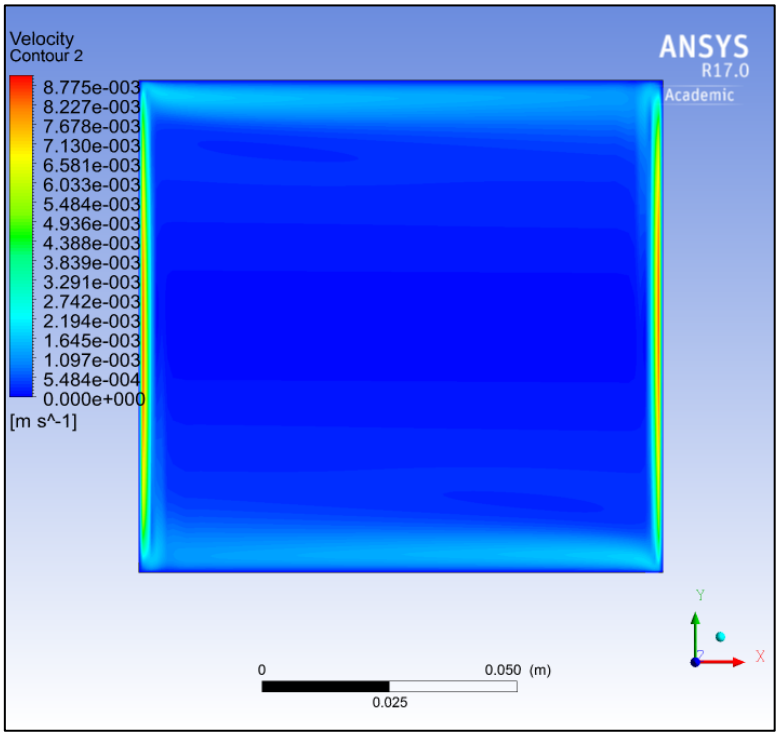

Figure 24: Velocity contour plot for volume fraction 0.05%

The contour plots above perfectly depict the buoyancy-driven natural convection that is expected in the case of a cavity with two opposite walls of a constant temperature.

The following graph depicts a comparison of the results obtained from the numerical investigation and those obtained from the experimental investigation.

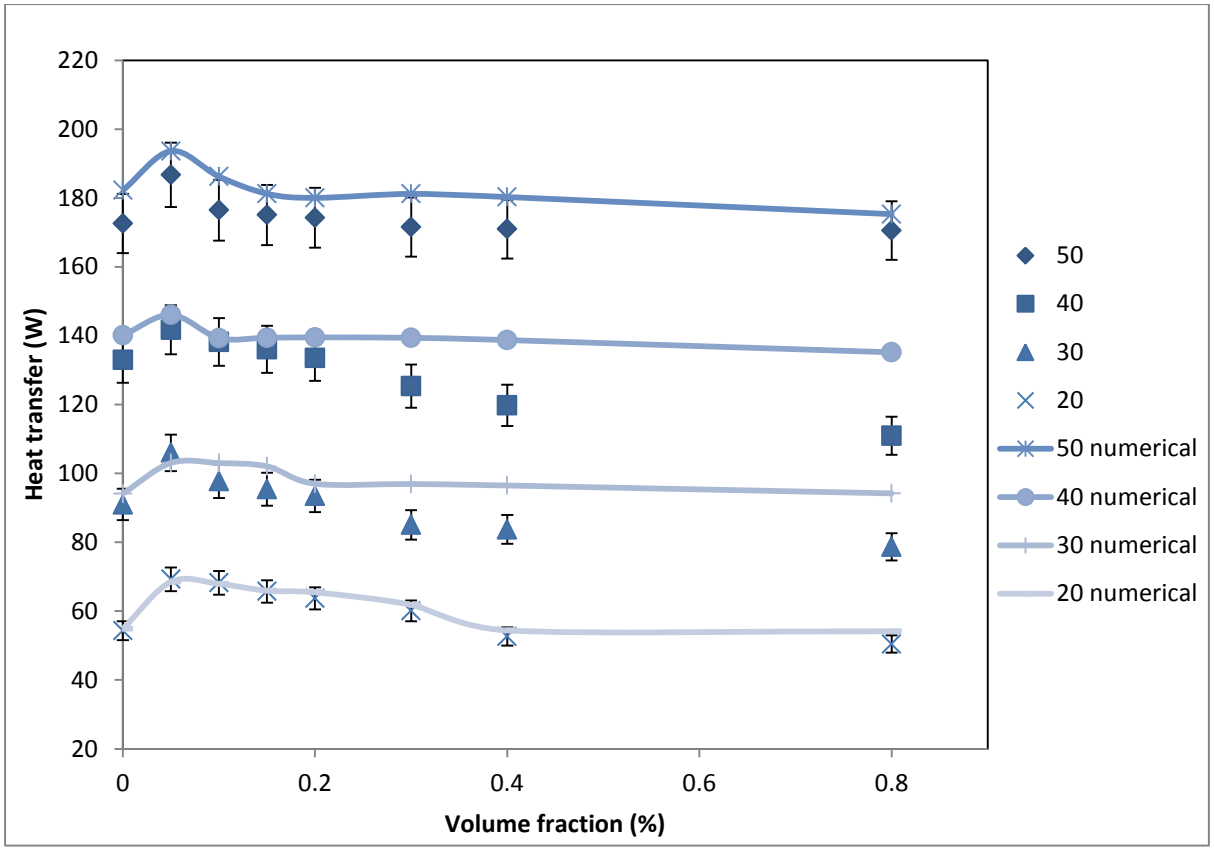

Figure 25: Heat transfer vs volume fraction for various temperature differences (experimental and numerical results)

From the heat transfer vs volume fraction graph above (Figure 25), it is clear that the numerical and experimental investigations show good correlation between the results. The difference in the results of the two different investigations is more pertinent for higher volume fractions, while the difference between the two is insignificant for volume fractions lower than 0.2%.

4.11 Conclusion and recommendations of the numerical investigation

This section summarises the numerical investigation and provides a conclusion, as well as recommendations made by the author.

4.11.1 Conclusion of the numerical investigation

A numerical investigation is performed using the CFD software ANSYS-FLUENT. The experimental cavity is modelled in two dimensions using the middle cross-section of the cavity. The simulation is set up as suggested in a tutorial made available by the software developers.

The mesh used in the simulations is validated by proving that the solution is not dependent on the mesh size. The mesh quality is also checked to allow for an accurate solution.

The same cases that were investigated experimentally were modelled numerically.

As a next step, the results from the numerical investigation are validated. This is done by comparing the results of the numerical investigation to those of the experimental investigation. The results for 0 0.002 volume fraction are chosen as comparison points. It is found that very little difference exists

between the results, with the percentage difference remaining below 4.5%. The highest percentage difference between the experimental and numerical results can be found at the higher temperature differences. This is due to the fact that the heat losses (which are not taken into account in the numerical modelling) increase as the average temperature increases. It is concluded that the error is small enough to be considered insignificant.

The overall numerical results were then analysed and compared to the experimental results. The same conclusions were drawn from both the numerical and the experimental results: the maximum heat transfer takes place at a temperature difference of 50 °C with the nanofluid with a volume fraction of 0.005.

4.11.2 Recommendations made from the numerical investigation

It is recommended that the particle size, dimensions of the cavity and particle material are varied to investigate the dependency of the heat transfer on these elements.

5. Conclusion and recommendations of the investigation

The complete investigation is summarised by the author and conclusions are drawn. From these conclusions, the author provides recommendations.

5.1 Conclusion of the investigation

For this Master of Engineering study, an experimental and numerical investigation into the heat transfer capabilities and thermophysical properties of a nanofluid in a cavity with opposite heated and cooled walls was performed.

A detailed literature study was undertaken on nanofluids and natural convection in these nanofluids. The existing models used to predict the thermophysical properties of nanofluids and the heat transfer through nanofluids were discussed. Past investigations of such nanofluids were summarised. These investigations can be divided into experimental, numerical and theoretical investigations, with the focus of this study falling on experimental and numerical investigations. The literature review also focused on work already completed in the field of natural convection or buoyancy-driven heat transfer through nanofluids in cavities.

From the extensive literature study, a nanofluid was selected for the experimental and numerical investigations of this study, tested at various volume fractions of TiO_2 nanoparticles in deionised water.

The experimental investigation was designed and performed. It incorporated various stable volume fractions and temperature differences to allow for an overview of the TiO_2 nanofluid. Safety was taken into account and investigated in detail during the study, as the effects of nanofluids on humans and the environment are not yet known. Precautions were taken to ensure safety during the investigation.

The results obtained from the experimental investigation were analysed and explained. Heat transfer was found to increase with an increase in the temperature difference, and the optimum volume percentage was found to be 0.05%. At this volume fraction and a temperature difference of 50 °C, the heat transfer was at a maximum of 186.76 W, which was a 8.2% increase on heat transfer through pure deionised water.

In the numerical investigation that followed, the CFD software ANSYS-FLUENT and the experimentally determined thermophysical properties of the nanofluid were utilised to perform the same investigation numerically. The experimental cavity was modelled in two dimensions as a cross-section of the experimental cavity. The same cases were also modelled as investigated in the experimental study. A quality-checked and independent mesh was used to perform the simulation.

The simulations produced results that were then compared to those of the experimental study to validate both the experimental results and the numerical models used. The results showed similarities with small differences occurring at the higher volume fractions and at higher temperature differences. These errors could be explained by the heat losses experienced in the experimental investigation that were not included in the numerical model.

Due to the good correlation between the experimental and numerical investigation, the results from the study can be accepted.

5.2 Recommendations made from the investigation

From the conclusions drawn about the study, several recommendations are made by the author.

It is recommended that the experimental and numerical investigations are extended to include various particle sizes, as well as different particle materials (such as copper, aluminium and platinum). This would allow for an investigation into the dependency of the heat transfer enhancement on both the particle size and the material suspended in the base fluid.

The variation of the distance between the two heated walls would also allow for an investigation into the effect that this change would have on heat transfer through the fluid. The effect of the overall geometry and size of the cavity should also be investigated by varying the dimensions of the cavity.

The implementation of the recommendations would allow for a more extensive study and could produce valuable information.

The final conclusion of the study is that the heat transfer of deionised water is enhanced by up to 8.2% through the suspension of TiO_2 particles in it. Through further investigation, this heat transfer enhancement can be used to optimise heat exchanger application.

Bibliography

1. Cengel, Y.A.G., Afshin J., *Heat and Mass Transfer, Fundamentals and Applications*. 4 ed. 2011.
2. Aybar, H.Ş., M. Sharifpur, M.R. Azizian, M. Mehrabi, and J.P. Meyer, *A Review of Thermal Conductivity Models for Nanofluids.* Heat Transfer Engineering, 2015. **36**(13): p. 1085-1110.
3. Meyer, J.P., S.A. Adio, M. Sharifpur, and P.N. Nwosu, *The Viscosity of Nanofluids: A Review of the Theoretical, Empirical, and Numerical Models.* Heat Transfer Engineering, 2015. **37**(5): p. 387-421.
4. Einstein, A., *A new determination of molecular dimensions.* Ann. Phys, 1906. **19**(2): p. 289-306.
5. Smoluchowski, M.V., *Theoretische Bemerkungen über die Viskosität der Kolloide.* Kolloidzschr, 1916. **80**: p. 190-195.
6. Booth, F. *The electroviscous effect for suspensions of solid spherical particles*. in *Proceedings of the Royal Society of London A: Mathematical, Physical and Engineering Sciences*. 1950. The Royal Society.
7. Bull, H.B., *The electroviscous effect in egg albumin solutions.* Transactions of the Faraday Society, 1940. **35**: p. 80-84.
8. Taylor, G.I., *The viscosity of a fluid containing small drops of another fluid.* Proceedings of the Royal Society of London. Series A, Containing Papers of a Mathematical and Physical Character, 1932: p. 41-48.
9. Vand, V., *Viscosity of solutions and suspensions. I. Theory.* The Journal of Physical Chemistry, 1948. **52**(2): p. 277-299.
10. Brinkman, H., *The viscosity of concentrated suspensions and solutions.* The Journal of Chemical Physics, 1952. **20**(4): p. 571-571.
11. Mooney, M., *The viscosity of a concentrated suspension of spherical particles.* Journal of colloid science, 1951. **6**(2): p. 162-170.
12. Roscoe, R., *The viscosity of suspensions of rigid spheres.* British Journal of Applied Physics, 1952. **3**(8): p. 267.
13. Batchelor, G., *The effect of Brownian motion on the bulk stress in a suspension of spherical particles.* Journal of Fluid Mechanics, 1977. **83**(01): p. 97-117.
14. Krieger, I.M. and T.J. Dougherty, *A mechanism for non-Newtonian flow in suspensions of rigid spheres.* Trans. Soc. Rheol, 1959. **3**(1): p. 137-152.
15. Lundgren, T.S., *Slow flow through stationary random beds and suspensions of spheres.* Journal of Fluid Mechanics, 1972. **51**(02): p. 273-299.
16. Graham, A.L., *On the viscosity of suspensions of solid spheres.* Applied Scientific Research, 1981. **37**(3-4): p. 275-286.
17. Saitô, N., *Concentration dependence of the viscosity of high polymer solutions. I.* Journal of the Physical Society of Japan, 1950. **5**(1): p. 4-8.
18. Hatschek, E., *The general theory of viscosity of two-phase systems.* Transactions of the Faraday Society, 1913. **9**: p. 80-92.
19. Thomas, C.U. and M. Muthukumar, *Three-body hydrodynamic effects on viscosity of suspensions of spheres.* The Journal of chemical physics, 1991. **94**(7): p. 5180-5189.
20. Frankel, N. and A. Acrivos, *On the viscosity of a concentrated suspension of solid spheres.* Chemical Engineering Science, 1967. **22**(6): p. 847-853.
21. Chen, H., Y. Ding, and C. Tan, *Rheological behaviour of nanofluids.* New journal of physics, 2007. **9**(10): p. 367.
22. Masoud Hosseini, S., A. Moghadassi, and D. Henneke, *A new dimensionless group model for determining the viscosity of nanofluids.* Journal of Thermal Analysis and Calorimetry, 2010. **100**(3): p. 873-877.

23. Masoumi, N., N. Sohrabi, and A. Behzadmehr, *A new model for calculating the effective viscosity of nanofluids.* Journal of Physics D: Applied Physics, 2009. **42**(5): p. 055501.
24. Graf, W.H., *Hydraulics of sediment transport*. 1984: Water Resources Publication.
25. Avsec, J. and M. Oblak, *The calculation of thermal conductivity, viscosity and thermodynamic properties for nanofluids on the basis of statistical nanomechanics.* International Journal of Heat and Mass Transfer, 2007. **50**(21): p. 4331-4341.
26. Keblinski, P., S. Phillpot, S. Choi, and J. Eastman, *Mechanisms of heat flow in suspensions of nano-sized particles (nanofluids).* International journal of heat and mass transfer, 2002. **45**(4): p. 855-863.
27. Xuan, Y., Q. Li, and W. Hu, *Aggregation structure and thermal conductivity of nanofluids.* AIChE Journal, 2003. **49**(4): p. 1038-1043.
28. Das, S.K., N. Putra, P. Thiesen, and W. Roetzel, *Temperature dependence of thermal conductivity enhancement for nanofluids.* Journal of Heat Transfer, 2003. **125**(4): p. 567-574.
29. Jang, S.P. and S.U. Choi, *Role of Brownian motion in the enhanced thermal conductivity of nanofluids.* Applied physics letters, 2004. **84**(21): p. 4316-4318.
30. Bhattacharya, P., S. Saha, A. Yadav, P. Phelan, and R. Prasher, *Brownian dynamics simulation to determine the effective thermal conductivity of nanofluids.* Journal of Applied Physics, 2004. **95**(11): p. 6492-6494.
31. Kumar, D.H., H.E. Patel, V.R. Kumar, T. Sundararajan, T. Pradeep, and S.K. Das, *Model for heat conduction in nanofluids.* Physical Review Letters, 2004. **93**(14): p. 144301.
32. Koo, J. and C. Kleinstreuer, *A new thermal conductivity model for nanofluids.* Journal of Nanoparticle Research, 2004. **6**(6): p. 577-588.
33. Koo, J. and C. Kleinstreuer, *Impact analysis of nanoparticle motion mechanisms on the thermal conductivity of nanofluids.* International Communications in Heat and Mass Transfer, 2005. **32**(9): p. 1111-1118.
34. Prasher, R., P. Bhattacharya, and P.E. Phelan, *Thermal conductivity of nanoscale colloidal solutions (nanofluids).* Physical review letters, 2005. **94**(2): p. 025901.
35. Chon, C.H., K.D. Kihm, S.P. Lee, and S.U. Choi, *Empirical correlation finding the role of temperature and particle size for nanofluid (Al2O3) thermal conductivity enhancement.* Applied Physics Letters, 2005. **87**(15): p. 153107-153107.
36. Ren, Y., H. Xie, and A. Cai, *Effective thermal conductivity of nanofluids containing spherical nanoparticles.* Journal of Physics D: Applied Physics, 2005. **38**(21): p. 3958.
37. Prasher, R., P. Bhattacharya, and P.E. Phelan, *Brownian-motion-based convective-conductive model for the effective thermal conductivity of nanofluids.* Journal of heat transfer, 2006. **128**(6): p. 588-595.
38. Xu, J., B. Yu, M. Zou, and P. Xu, *A new model for heat conduction of nanofluids based on fractal distributions of nanoparticles.* Journal of Physics D: Applied Physics, 2006. **39**(20): p. 4486.
39. Evans, W., J. Fish, and P. Keblinski, *Role of Brownian motion hydrodynamics on nanofluid thermal conductivity.* Applied Physics Letters, 2006. **88**(9): p. 093116.
40. Vladkov, M. and J.-L. Barrat, *Modeling transient absorption and thermal conductivity in a simple nanofluid.* Nano letters, 2006. **6**(6): p. 1224-1228.
41. Yu-Hua, L., Q. Wei, and F. Jian-Chao, *Temperature dependence of thermal conductivity of nanofluids.* Chinese Physics Letters, 2008. **25**(9): p. 3319.
42. Shukla, R.K. and V.K. Dhir, *Effect of Brownian motion on thermal conductivity of nanofluids.* Journal of Heat Transfer, 2008. **130**(4): p. 042406.
43. Yang, B., *Thermal conductivity equations based on Brownian motion in suspensions of nanoparticles (nanofluids).* Journal of Heat Transfer, 2008. **130**(4): p. 042408.
44. Nie, C., W. Marlow, and Y. Hassan, *Discussion of proposed mechanisms of thermal conductivity enhancement in nanofluids.* International Journal of Heat and Mass Transfer, 2008. **51**(5): p. 1342-1348.

45. Vasu, V., K.R. Krishna, and A. Kumar, *Analytical prediction of thermophysical properties of fluids embedded with nanostructured materials.* International Journal of Nanoparticles, 2008. **1**(1): p. 32-49.
46. Jain, S., H.E. Patel, and S.K. Das, *Brownian dynamic simulation for the prediction of effective thermal conductivity of nanofluid.* Journal of Nanoparticle Research, 2009. **11**(4): p. 767-773.
47. Jung, J.-Y. and J.Y. Yoo, *Thermal conductivity enhancement of nanofluids in conjunction with electrical double layer (EDL).* International Journal of Heat and Mass Transfer, 2009. **52**(1): p. 525-528.
48. Murshed, S., K. Leong, and C. Yang, *A combined model for the effective thermal conductivity of nanofluids.* Applied Thermal Engineering, 2009. **29**(11): p. 2477-2483.
49. Xiao, B., Y. Yang, and L. Chen, *Developing a novel form of thermal conductivity of nanofluids with Brownian motion effect by means of fractal geometry.* Powder Technology, 2013. **239**: p. 409-414.
50. Yu, W. and S. Choi, *The role of interfacial layers in the enhanced thermal conductivity of nanofluids: a renovated Maxwell model.* Journal of Nanoparticle Research, 2003. **5**(1-2): p. 167-171.
51. Feng, Y., B. Yu, P. Xu, and M. Zou, *The effective thermal conductivity of nanofluids based on the nanolayer and the aggregation of nanoparticles.* Journal of Physics D: Applied Physics, 2007. **40**(10): p. 3164.
52. Yu, W. and S. Choi, *The role of interfacial layers in the enhanced thermal conductivity of nanofluids: a renovated Hamilton–Crosser model.* Journal of Nanoparticle Research, 2004. **6**(4): p. 355-361.
53. Xue, Q.-Z., *Model for effective thermal conductivity of nanofluids.* Physics letters A, 2003. **307**(5): p. 313-317.
54. Xie, H., M. Fujii, and X. Zhang, *Effect of interfacial nanolayer on the effective thermal conductivity of nanoparticle-fluid mixture.* International Journal of Heat and Mass Transfer, 2005. **48**(14): p. 2926-2932.
55. Leong, K., C. Yang, and S. Murshed, *A model for the thermal conductivity of nanofluids–the effect of interfacial layer.* Journal of nanoparticle research, 2006. **8**(2): p. 245-254.
56. Tillman, P. and J.M. Hill, *Determination of nanolayer thickness for a nanofluid.* International Communications in Heat and Mass Transfer, 2007. **34**(4): p. 399-407.
57. Zhou, X. and L. Gao, *Thermal conductivity of nanofluids: Effects of graded nanolayers and mutual interaction.* Journal of Applied Physics, 2008. **103**(8): p. 083503.
58. Wang, B.-X., L.-P. Zhou, and X.-F. Peng, *A fractal model for predicting the effective thermal conductivity of liquid with suspension of nanoparticles.* International Journal of Heat and Mass Transfer, 2003. **46**(14): p. 2665-2672.
59. Karthikeyan, N., J. Philip, and B. Raj, *Effect of clustering on the thermal conductivity of nanofluids.* Materials Chemistry and Physics, 2008. **109**(1): p. 50-55.
60. Prasher, R., W. Evans, P. Meakin, J. Fish, P. Phelan, and P. Keblinski, *Effect of aggregation on thermal conduction in colloidal nanofluids.* Applied Physics Letters, 2006. **89**(14): p. 143119.
61. Avsec, J., *The combined analysis of phonon and electron heat transfer mechanism on thermal conductivity for nanofluids.* International Journal of Heat and Mass Transfer, 2008. **51**(19): p. 4589-4598.
62. Corcione, M., *Rayleigh-Bénard convection heat transfer in nanoparticle suspensions.* International Journal of Heat and Fluid Flow, 2011. **32**(1): p. 65-77.
63. Corcione, M., *Empirical correlating equations for predicting the effective thermal conductivity and dynamic viscosity of nanofluids.* Energy Conversion and Management, 2011. **52**(1): p. 789-793.
64. Nabi, S. and E. Shirani, *Simultaneous effects of brownian motion and clustering of nanoparticles on thermal conductivity of nanofluids.* Iranian Journal of Science & Technology, Transactions of Mechanical Engineering, 2012. **36**(M1): p. 53-68.

65. Ho, C., W. Liu, Y. Chang, and C. Lin, *Natural convection heat transfer of alumina-water nanofluid in vertical square enclosures: an experimental study.* International Journal of Thermal Sciences, 2010. **49**(8): p. 1345-1353.
66. Sharifpur, M., S. Yousefi, and J.P. Meyer, *A new model for density of nanofluids including nanolayer.* International Communications in Heat and Mass Transfer, 2016. **78**: p. 168-174.
67. Ho, C., D.-S. Chen, W.-M. Yan, and O. Mahian, *Buoyancy-driven flow of nanofluids in a cavity considering the Ludwig–Soret effect and sedimentation: Numerical study and experimental validation.* International Journal of Heat and Mass Transfer, 2014. **77**: p. 684-694.
68. Chein, R. and J. Chuang, *Experimental microchannel heat sink performance studies using nanofluids.* International Journal of Thermal Sciences, 2007. **46**(1): p. 57-66.
69. Rao, S.S. and A. Srivastava, *Interferometric study of natural convection in a differentially-heated cavity with Al 2 O 3–water based dilute nanofluids.* International Journal of Heat and Mass Transfer, 2016. **92**: p. 1128-1142.
70. Rao, S.S. and A. Srivastava, *Interferometry-based whole field investigation of heat transfer characteristics of dilute nanofluids.* International Journal of Heat and Mass Transfer, 2014. **79**: p. 166-175.
71. Afifah, A., S. Syahrullail, and C.N. Azwadi, *NATURAL CONVECTION OF ALUMINIUM OXIDE-WATER NANOFLUID.* Jurnal Teknologi, 2015. **75**(11).
72. Putra, N., W. Roetzel, and S.K. Das, *Natural convection of nano-fluids.* Heat and Mass Transfer, 2003. **39**(8-9): p. 775-784.
73. Jahanshahi, M., S. Hosseinizadeh, M. Alipanah, A. Dehghani, and G. Vakilinejad, *Numerical simulation of free convection based on experimental measured conductivity in a square cavity using water/SiO 2 nanofluid.* International communications in heat and mass transfer, 2010. **37**(6): p. 687-694.
74. Heris, S.Z., M.B. Pour, O. Mahian, and S. Wongwises, *A comparative experimental study on the natural convection heat transfer of different metal oxide nanopowders suspended in turbine oil inside an inclined cavity.* International Journal of Heat and Mass Transfer, 2014. **73**: p. 231-238.
75. Yu, Z.-T., W. Wang, X. Xu, L.-W. Fan, Y.-C. Hu, and K.-F. Cen, *A numerical investigation of transient natural convection heat transfer of aqueous nanofluids in a differentially heated square cavity.* International Communications in Heat and Mass Transfer, 2011. **38**(5): p. 585-589.
76. Ternik, P., *Conduction and convection heat transfer characteristics of water–Au nanofluid in a cubic enclosure with differentially heated side walls.* International Journal of Heat and Mass Transfer, 2015. **80**: p. 368-375.
77. He, Y., C. Qi, Y. Hu, B. Qin, F. Li, and Y. Ding, *Lattice Boltzmann simulation of alumina-water nanofluid in a square cavity.* Nanoscale research letters, 2011. **6**(1): p. 1-8.
78. Fattahi, E., M. Farhadi, K. Sedighi, and H. Nemati, *Lattice Boltzmann simulation of natural convection heat transfer in nanofluids.* International journal of thermal sciences, 2012. **52**: p. 137-144.
79. Sajjadi, H., M. Gorji, G. Kefayati, and D. Ganji, *Lattice Boltzmann simulation of turbulent natural convection in tall enclosures using Cu/water nanofluid.* Numerical Heat Transfer, Part A: Applications, 2012. **62**(6): p. 512-530.
80. Corcione, M., M. Cianfrini, and A. Quintino, *Enhanced natural convection heat transfer of nanofluids in enclosures with two adjacent walls heated and the two opposite walls cooled.* International Journal of Heat and Mass Transfer, 2015. **88**: p. 902-913.
81. Alinia, M., M. Gorji-Bandpy, D. Ganji, S. Soleimani, E. Ghasemi, and A. Darvan, *Two-phase natural convection of SiO^ sub 2^-water nano fluid in an inclined square enclosure.* Scientia Iranica. Transaction B, Mechanical Engineering, 2014. **21**(5): p. 1643.
82. Abouali, O. and A. Falahatpisheh, *Numerical investigation of natural convection of Al2O3 nanofluid in vertical annuli.* Heat and mass transfer, 2009. **46**(1): p. 15-23.

83. Sheikhzadeh, G.A., M. Dastmalchi, and H. Khorasanizadeh, *Effects of nanoparticles transport mechanisms on Al 2 O 3–water nanofluid natural convection in a square enclosure.* International Journal of Thermal Sciences, 2013. **66**: p. 51-62.
84. Cianfrini, C., M. Corcione, E. Habib, and A. Quintino, *Buoyancy-induced convection in/water nanofluids from an enclosed heater.* European Journal of Mechanics-B/Fluids, 2014. **48**: p. 123-134.
85. Moradi, H., B. Bazooyar, S.G. Etemad, and A. Moheb, *Influence of the geometry of cylindrical enclosure on natural convection heat transfer of Newtonian nanofluids.* Chemical Engineering Research and Design, 2015. **94**: p. 673-680.
86. Hu, Y., Y. He, S. Wang, Q. Wang, and H.I. Schlaberg, *Experimental and numerical investigation on natural convection heat transfer of TiO2–water nanofluids in a square enclosure.* Journal of Heat Transfer, 2014. **136**(2): p. 022502.
87. Ganji, D. and A. Malvandi, *Natural convection of nanofluids inside a vertical enclosure in the presence of a uniform magnetic field.* Powder Technology, 2014. **263**: p. 50-57.
88. Sheikholeslami, M., H. Ashorynejad, and P. Rana, *Lattice Boltzmann simulation of nanofluid heat transfer enhancement and entropy generation.* Journal of Molecular Liquids, 2016. **214**: p. 86-95.
89. Ouyahia, S.-E., Y.K. Benkahla, and N. Labsi, *Numerical Study of the Hydrodynamic and Thermal Proprieties of Titanium Dioxide Nanofluids Trapped in a Triangular Geometry.* Arabian Journal for Science and Engineering, 2016. **41**(5): p. 1995-2009.
90. Buongiorno, J., *Convective transport in nanofluids.* Journal of Heat Transfer, 2006. **128**(3): p. 240-250.
91. Sheikholeslami, M., M. Gorji-Bandpay, and D. Ganji, *Magnetic field effects on natural convection around a horizontal circular cylinder inside a square enclosure filled with nanofluid.* International Communications in Heat and Mass Transfer, 2012. **39**(7): p. 978-986.
92. He, Y., Y. Men, Y. Zhao, H. Lu, and Y. Ding, *Numerical investigation into the convective heat transfer of TiO 2 nanofluids flowing through a straight tube under the laminar flow conditions.* Applied Thermal Engineering, 2009. **29**(10): p. 1965-1972.
93. Limited, A.D.C., *SV-10/SV-100 Vibro Viscometer Instruction Manual*. 2008: A&D Company Limited.
94. Mahdavi, M., H. Ghodsinezhad, M. Sharifpur, and J. Meyer, *BOUNDARY CONDITION INVESTIGATION FOR CAVITY FLOW NATURAL CONVECTION.*